MAPPING SURFICIAL MATERIALS IN NUNAVUT USING RADARSAT-2 C-HH AND C-HV, LANDSAT-8 OLI, DEM AND SLOPE DATA

by

Justin Thomas Bezanson Byatt

BSc Environmental Management, University of New Brunswick, 2014

A Thesis Submitted in Partial Fulfillment of
the Requirements for the Degree of

Master of Science in Forestry

In the Graduate Academy Unit of
Forestry and Environmental Management

Supervisors:	Brigitte Leblon, PhD, Forestry and Environmental Management Armand LaRocque, PhD, Forestry and Environmental Management
Advisory Committee:	Jeff Harris, PhD Isabelle McMartin, PhD, Geological Survey of Canada
Examining Board:	Fan-Rui Meng, PhD, Forestry and Environmental Management Emmanuel Stefenakis, PhD, GGE

This thesis is accepted by the
Dean of Graduate Studies

THE UNIVERSITY OF NEW BRUNSWICK

May, 2017

ABSTRACT

The Canadian Arctic is currently the focus of increased mapping activities, which aim to provide better knowledge to assist in making informed decisions for sustainable minerals and energy development, and land-use management. One of the required maps deals with surficial materials. This thesis studies the potential of combining RADARSAT-2 SAR images with Landsat-8 optical data, DEM and slope data to map surficial materials in the region around Wager Bay, Nunavut. Two study areas were selected, one on the northern side of the bay (NTS map areas 046E, K, L, M, 056H, I, J) and another one on the southern side (NTS map sheets 046D, E, 055P, 056A, H). The images were classified using a non-parametric classifier Random Forests. The results show that including RADARSAT-2 images in the classification process increases the overall classification accuracy from 92.8% to 98.1% in the north region and 96.7% to 99.3% in the south region. The classified maps were compared to GPS data sets to determine the mapping accuracy, and there was a similar increase in accuracy when RADARSAT-2 data was added. The limitations of the study are also presented, as well as potential improvements.

Key words: surficial materials, remote sensing, SAR, RADARSAT-2, Landsat, optical, Arctic mapping.

AKNOWLEDGMENTS

J. Byatt is funded by a scholarship from NSERC, NBIF, and ACUNS (with the help from the W Garfield Weston Foundation) and by a NSERC Discovery Grant awarded to Dr. Brigitte Leblon. The field work was funded by the Natural Resources Canada's Geo-mapping for Energy and Minerals (GEM-1&2) program, as part of the GEM-2 Tehery-Wager Activity within the Rae Project area. The RADARSAT-2 images were provided to the UNB team by the Canadian Space Agency via the Geological Survey of Canada. Thanks to Deborah Lemkow (GSC) for helping with RADARSAT-2 image ordering and the anonymous reviewers. Thank you to my supervisors, B. Leblon, and A. LaRocque, and the Advisory Committee Members, I. McMartin, and J. Harris. I would also like to thank my parents and family, and my partner Scott for their continued support.

TABLE OF CONTENTS

LIST OF TABLES

LIST OF FIGURES

Figure **Page**

LIST OF ACRONYMS

amsl	Above mean sea level
GCP	Ground Control Point
GPS	Global Positioning System
LST	Local Standard Time
RMS	Root Mean Square error
SAR	Synthetic Aperture Radar

CHAPTER 1

INTRODUCTION

The Canadian Arctic presents unique challenges in mapping surficial materials. It is a vast region, sparsely populated with harsh environmental conditions. These circumstances make it very difficult for traditional methods of mapping of surficial materials, which require extensive and costly field surveys. Accurate maps can take years to make, and be expensive to produce. Remote predictive mapping can offer assistance in this process, reducing field surveys and improving accuracy. Satellite data is easily available, relatively cheap, and can be processed year round. It can also cover a large region faster than traditional ground surveys.

Different types of satellite data have been used in remote predictive mapping. The use of optical data from Landsat satellites has been tested for mapping surficial materials in the Arctic. However, the resulting map has a low mapping accuracy. In several studies (Grunsky et al., 2009; Mei and Paulen, 2009; Shelat et al., 2012; LaRocque et al., 2012), adding synthetic aperture radar (SAR) data in the classification led to an increase of the mapping accuracy. Indeed, SAR images are highly complementary to optical images. SAR images are sensitive to surface texture by providing information on scattering mechanisms that are related to surface roughness and moisture content (Harris et al., 2008; LaRocque et al., 2012). Optical images are sensitive to surficial reflective properties that are generally governed by surface chemistry, vegetation, and surface moisture content (Brown et al., 2008).

This thesis will make use of Landsat 8 OLI optical images and RADARSAT-2 SAR C-HH and C-HV images combined with a digital elevation model (DEM) and derived slope data for producing maps of more than 20 surficial material classes around Wager Bay in Nunavut. It is part of a surficial geology mapping effort funded by Natural Resources Canada's Geo-mapping for Energy and Minerals (GEM) program to provide new geological knowledge on the nature and composition of surficial materials for sustainable management and development in central mainland Nunavut (McMartin et al., 2015a, b; McMartin et al., 2016).

Using only Landsat-7 ETM+ images, Campbell et al. (2013) mapped 12 classes of surficial materials in an area located north of Wager Bay and Wityk et al (2013) were able to map 15 classes of surficial materials in an area west of Repulse Bay. However, the classification overall accuracy was approximately 60% in both of these cases. We hypothesized that the mapping accuracy will increase by adding SAR C-HH and C-VV images from RADARSAT-2.

In both Campbell et al. (2013) and Wityk et al (2013), such as in the other studies on surficial deposit mapping in the Arctic (Grunsky et al., 2009; Mei and Paulen, 2009; Shelat et al., 2012; LaRocque et al., 2012), the maps were produced by applying a supervised maximum likelihood classifier (MLC). This parametric classifier has recently been shown to be less effective than the non-parametric supervised classifier, *Random Forests (RF)*, for surficial material mapping in Nunavut with RADARSAT-2 and Landsat-7 ETM+ data (LaRocque et al., 2013) and for land cover mapping in New

Brunswick with RADARSAT-2, ALOS-PALSAR and Landsat-7 ETM+ data (LaRocque et al., 2014). Also, RF can use both Gaussian and non-Gaussian data and can handle more input datasets.

This thesis is a paper-based format, composed of 2 papers related to the surficial material map in the region surrounding Wager Bay, Nunavut (Chapters 2 and 3). In Chapter 2, we produce a map with 21 surficial material classes for an area located north of Wager Bay (NTS map areas 46E, K, L, M, 56H, I, J), covering the same area as Campbell et al. (2013). Chapter 3 presents a map with 22 surficial material classes for an area located south of Wager Bay (NTS map sheets 46E, D, 55P, 56A, H). Both maps provide a first order assessment of the surface materials of the region, and test the effectiveness of applying *Random Forests* classifier to a combination of RADARSAT-2 SAR imagery with Landsat-8 optical imagery. Both papers will be submitted to International Journal of Remote Sensing with the following authorship

1. Byatt, J., LaRocque, A., Leblon, B., Harris, J., and McMartin, I. 2017. Mapping surficial materials in Nunavut using RADARSAT-2 C-HH and C-HV, Landsat-8 OLI, DEM, and slope data. Part 1 - North of Wager Bay area, International Journal of Remote Sensing (submitted)
2. Byatt, J., LaRocque, A., Leblon, B., Harris, J., and McMartin, I. 2017. Mapping surficial materials in Nunavut using RADARSAT-2 C-HH and C-HV, Landsat-8 OLI, DEM, and slope data. Part 2 - South of Wager Bay area, International Journal of Remote Sensing (submitted)

REFERENCES

Brown, O., Harris, J.R., and Utting, D. 2008: Case study 6: surficial mapping of northern Baffin Island using Landsat and topographic data; *in* Remote Predictive Mapping: An Aid for Northern Mapping, J.R. Harris (ed.), Geological Survey of Canada, Open File 5643, p. 225–232.

Campbell, J.E., Harris, J.R., Huntley, D.H., McMartin, I., Wityk, U., Dredge, L.A., and Eagles, S. 2013: Remote predictive mapping of surficial earth materials: Wager Bay north area, Nunavut - NTS 46-E (N), 46-K (SW), 46-L, 46-M (SW), 56-H (N), 56-I and 56-J (S); Geological Survey of Canada, Open File 7118, 42 p.

Grunsky, E., Harris, J.R., and McMartin, I. 2009: Predictive mapping of surficial materials, Schultz Lake area (NTS 66 A), Nunavut, Canada; Reviews in Economic Geology, 16, 177–198.

Harris, J.R., Grunsky, E., and McMartin, I. 2008: Classification of remotely sensed imagery for surficial geological mapping in Canada's north, Case 7; in Remote Predictive Mapping: An Aid for Northern Mapping, J.R. Harris (ed.), Geological Survey of Canada, Open File 5643, p. 233–244.

LaRocque, A., Leblon, B., Harris, J.R., Jefferson, C.W., Tschirhart, V., and Shelat, Y. 2012: Surficial materials mapping in Nunavut, Canada, with multi-beam RADARSAT-2 dual-polarization C-HH and C-HV, Landsat-7 ETM+, and DEM data; Canadian Journal of Remote Sensing, 38, 281–305.

LaRocque, Armand, Brigitte Leblon, Renata Woodward; Michael Mordini, Laura Bourgeau-Chavez, Anthony Landon, Nancy French, Jessica McCarthy, Tom

Huntington, and Philip Camill (2014). Use of RADARSAT-2 and ALOS-PALSAR SAR images for wetland mapping in New Brunswick. Proceedings of the 2014 IEEE International Geoscience and Remote Sensing Symposium (IGARSS 2014) and of the 35th Canadian Symposium on Remote Sensing, Québec (QC): 1226-1229.

McMartin, I., Campbell, J.E., Dredge, L.A., LeCheminant, A.N., McCurdy, M.W., and Scromeda, N., 2015a. Quaternary geology and till composition north of Wager Bay, Nunavut: results from the GEM Wager Bay Surficial Geology Project; Geological Survey of Canada, Open File 7748, 58 p.

McMartin, I., Byatt, J., Randour, I., and Day, S.J.A., 2015b. Report of 2015 activities for regional surficial mapping, till and stream sediment sampling in the Tehery-Wager GEM 2 Rae Project area; Geological Survey of Canada, Open File 7966, 14 p.

McMartin, I., Day, S.J.A., Randour, I., Roy, M., Byatt, J., LaRocque, A., and Leblon, B., 2016. Report of 2016 activities for the surficial mapping and sampling surveys in the Tehery-Wager GEM-2 Rae Project area; Geological Survey of Canada, Open File 8134, 16p.

Mei, S., and Paulen, R.C. 2009: Using multi-beam RADARSAT-1 imagery to augment mapping surficial geology in northwest Alberta, Canada; Canadian Journal of Remote Sensing, 35, 1–22.

Shelat, Y., Leblon, B., LaRocque, A., Harris J., Jefferson, C. W., Lentz, D., and Tschirhart, V. 2012b. Effects of incidence angles and image combinations on mapping accuracy of surficial materials in the Umiujalik Lake area, Nunavut using

RADARSAT-2, polarimetric and Landsat 7 images, and DEM data. Part 1. Non-Polarimetric Analysis. Canadian Journal of Remote Sensing, 38(3): 383-403

Wityk, U., Harris, J.R., McMartin, I., Campbell, J.E., Ross, M., and Grunsky, E., 2013. Remote predictive mapping of surficial materials, West of Repulse Bay, Nunavut (NTS 46M-SW, 46L-W and -S, 46K-SW), GSC Open File 7357, 20 pages and appendice

CHAPTER 2
MAPPING SURFICIAL MATERIALS IN NUNAVUT USING RADARSAT-2 C-HH AND C-HV, Landsat-8 OLI, DEM AND SLOPE DATA. PART 1 - NORTH OF WAGER BAY AREA[1]

2.1 ABSTRACT

The Canadian Arctic is currently the focus of increased mapping activities, which aim to provide better knowledge to assist in making informed decisions for sustainable minerals and energy development, and land-use management. One of the types of maps required deals with surficial materials. In an area located north of Wager Bay, Nunavut (NTS map areas 46E, K, L, M, 56H, I, J), a map with 21 surficial material classes was produced using a non-parametric classifier, Random Forests (RF), applied to a combination of RADARSAT-2 C-band dual- polarized (HH and HV) and Landsat-8 OLI images with a digital elevation model and slope data. Two versions of Random Forests were tested: the *all-polygon* and the *sub-polygon* versions. The resulting map was compared to about 1000 GPS sites to determine its mapping accuracy. We showed that adding RADARSAT-2 C-HH and C-HV images to the classifier strongly improves the classification and mapping accuracy. The classification overall accuracy increases from 90.6% to 96.4% with the *sub-polygon* script and from 92.8% to 98.1% with the *all-polygon* script. Similarly, the mapping accuracy increases from 76.3% to 88.9% with the sub-polygon script and from 76.4% to 93.3% with the all-polygon script. With the *all-*

1. [1] Byatt, J., LaRocque, A., Leblon, B., Harris, J., and McMartin, I. 2017. Mapping surficial materials in Nunavut using RADARSAT-2 C-HH and C-HV, Landsat-8 OLI, DEM, and slope data. Part 1 - North of Wager Bay area, International Journal of Remote Sensing (submitted)

polygon script, both the user's and producer's accuracies for each individual class exceed 95%, with exception of six classes having user's accuracies higher than 89% (*sandy till (sT), gravelly till (gT),* and both *sand and gravel classes (SG and SGV)).* Similarly, the mapping user's and producer's accuracies are above 85% for all individual classes, except the user's accuracy of the *gravelly till (gT) class* (76.7%) and the producer's accuracy of the *sand and gravel with vegetation (SGV)* class (70%). In both cases, the confusion mainly occurred with *thin till over bedrock* (*T/R).* The limitations of the study are also presented.

2.2 INTRODUCTION

The Canadian Arctic is currently the focus of increased mapping activities, which aim to provide better knowledge to assist in making informed decisions for sustainable resource and infrastructure development, and land-use management. Northern Canada presents challenges for mapping because the land area is vast and difficult to access. Geological mapping has traditionally been done at a regional scale and accomplished by expensive and logistically challenging field programs. Remote predictive mapping (RPM) is a technique that can be used to map vast areas in a time-efficient manner and at a relatively low cost (Harris, 2008a). It uses satellite imagery and associated image processing technology to produce maps. Satellite imagery offers the advantages of extensive regional coverage, no disturbances to the area being mapped and a method of acquiring data in less accessible areas on a regular and cost-effective basis. In the case of surficial materials, remote predictive mapping provides a first-order assessment of the unconsolidated sediment covering the study area, guides geological mapping field

activities (both surficial and bedrock), assists in interpretation of the surficial geology between field sites, and provides a regional context for the surficial materials.

Remote predictive mapping can be performed using optical imagery such as the ones acquired by Landsat or SPOT satellites (Harris et al., 2011); however, optical images cannot be acquired at night or during cloudy conditions. Such limitations do not exist with synthetic aperture radar (SAR) images, such as the ones acquired by RADARSAT-2 (e.g., Schetselaar et al., 2007; LaRocque et al., 2012). Combining SAR and optical imagery offers several advantages because both image types are complementary (Grunsky et al., 2009; Mei and Paulen, 2009; Shelat et al., 2012; LaRocque et al., 2012). SAR images are sensitive to surface texture by providing information on scattering mechanisms that are related to surface roughness and moisture content (Harris et al., 2008b; LaRocque et al., 2012). Optical images are sensitive to surficial reflective properties that are generally governed by surface chemistry, vegetation, and surface moisture content (Brown et al., 2008).

Canada pioneered the building of two C-band radar satellites (RADARSAT-1 and RADARSAT-2) which provided multi-polarization options. RADARSAT images have been used to map surficial materials of specific regions of Canada's North, namely around Baker Lake (Nunavut), using HH images (e.g., Harris et al., 2008b; Grunsky et al., 2009), HH and HV images (LaRocque et al. 2012), and HH, HV, and VV images (Shelat et al. 2012). In these studies, SAR images were combined with Landsat-7 ETM+ images and a digital elevation model (DEM) and the classification accuracy was above 85%. However, these studies were only able to map 8 (or less) broad classes of surficial materials, namely bedrock, boulders, organic deposits, sand and gravel, thick till with

dense vegetation, thick till with sparse vegetation, and thin till. Using only Landsat-7 ETM+ images, Campbell et al. (2013) mapped 12 classes of surficial materials in an area located north of Wager Bay and Wityk et al (2013) were able to map 15 classes of surficial materials in an area west of Repulse Bay. However, the classification overall accuracy was approximately 60% in both of these cases.

All the aforementioned studies used the supervised maximum likelihood classifier (MLC). This parametric classifier has recently been shown to be less effective than the non-parametric supervised classifier, *Random Forests (RF)*, using RADARSAT-2 and Landsat-7 ETM+ data for surficial material mapping in Nunavut (LaRocque et al., 2013) and land cover mapping in New Brunswick (LaRocque et al., 2014). Also, RF can use both Gaussian and non-Gaussian data and can handle more input datasets.

This study assesses the use of Landsat 8 OLI optical images and RADARSAT-2 SAR C-HH and C-HV images combined with a digital elevation model (DEM) and derived slope data for producing maps of more than 20 surficial material classes around Wager Bay in Nunavut. It is part of a surficial geology mapping effort funded by Natural Resources Canada's Geo-mapping for Energy and Minerals (GEM) program to provide new geological knowledge on the nature and composition of surficial materials for sustainable management and development in central mainland Nunavut (McMartin et al., 2015a, b; McMartin et al., 2016).

The study is subdivided into two parts. In this paper (Part 1), we produce a map with 21 surficial material classes for an area located north of Wager Bay (NTS map areas 46E, K, L, M, 56H, I, J), covering the same area as Campbell et al. (2013). The second paper (Part 2) (Byatt et al. 2017) presents a map with 22 surficial material classes for an area

located south of Wager Bay (NTS map sheets 46E, D, 55P, 56A, H). In both papers, the maps were produced by applying the *Random Forest*™ supervised classifier to a combination of the images with a digital elevation model and slope data. We use a different approach than the one used by Campbell et al. (2013) because we use SAR images in addition to optical imagery. We also employ a more robust classification method (RF) to map more classes. In addition the resulting surficial material map is fully validated using an independent set of georeferenced field observation points.

2.3 STUDY AREA

The study area is located north of Wager Bay, Nunavut, on the northwestern side of Hudson Bay (86°-92° Long. W 65-67.5° Lat. N) and includes parts of Ukkusiksalik National Park (Figure 2.1). It covers the following NTS map sheets: 46E, 46K, 46L, 46M, 56H, 56I, 56J. The digital elevation model of Figure 2.1 shows that elevations range from sea level along Wager Bay and Hudson Bay to 627 m amsl in the northwestern part of the study area. The drainage network links numerous intermediate to large lakes and ponds, the biggest in the study area being Curtis Lake (Figure 2.1). The overall discharge direction of drainage systems is from west to east, either through Wager Bay and Repulse Bay into Hudson Bay, or curving north into Committee Bay and ultimately the Arctic Ocean. Records at one of the closest weather stations (Baker Lake, 64°19′05″N ,096°01′03″W) indicate that the monthly average maximum temperature is between +17° C and -29° C and the monthly average minimum temperature is between +6° and -36° C. These temperatures are suitable for the development of Arctic tundra vegetation that is composed of dwarf shrubs, birch, willow mixed with herbs, lichens, and mosses (Smith et al., 2004). Lowland areas are occupied by wetlands, which have

predominantly a thin organic cover (peat). Cryosols occupy large parts of this Arctic region, and are associated with deep permafrost (frozen soil) and related periglacial landforms (Smith et al., 2004). However, the top layer of ground frost thaws during the summer, creating pools of standing water and/or saturated soils. Standing water may cause specular reflection resulting in no backscatter. Saturated soils will generate more backscatter due to higher dielectric properties.

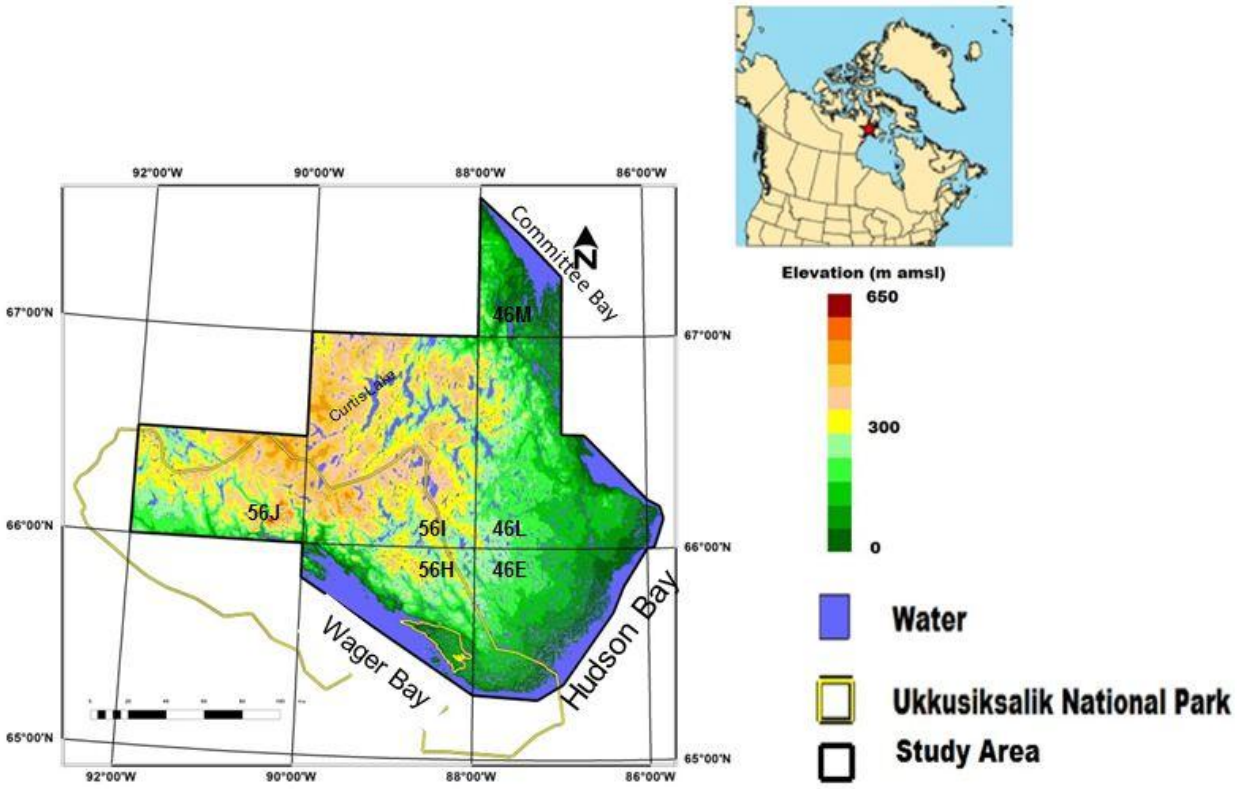

Figure 2.1. Location of the study area north of Wager Bay (Nunavut) and related digital elevation model and hydrographic network.

From a surficial geology point of view, the area is characterized by north-trending streamlined, thin and thick till extending from a major ice divide zone located south of Wager Bay (Keewatin Ice Divide), from which ice flowed radially during the last glaciation (McMartin et al. 2015a). An ice-flow reversal into Repulse Bay occurred during late deglaciation as evidenced by weakly fluted till to the east superimposed on

the prevailing north-trending landforms. This glacial landscape is interspersed by north-flowing and east-flowing subglacial meltwater corridors, and a profusion of proglacial and ice-marginal channels associated with a complex ice retreat pattern and remnant caps of cold-based ice. While boulder cover is variable on the till surfaces, it is quite dense (> 60%) in some areas, particularly where the till is thin or has been affected by meltwater erosion. The limit of postglacial marine inundation decreases from 240 m amsl west of Committee Bay to about 145 m amsl west of Repulse Bay and 130 m amsl at the mouth of Wager Bay. Lowlands that skirt the coasts of Repulse Bay and Hudson Bay show evidence for postglacial marine erosion and reworking of thin glacial and glaciofluvial sediments. In these lowlands, marine veneers are sandy and occur as scattered deposits between rock ridges or glacial landforms. Thick accumulations of marine silts and clays dominate the west coastal plain of Committee Bay in the north.

2.4 MATERIALS

We used ten Landsat-8 images acquired over three years from 2013 to 2015 by the *Operational Land Imager* (OLI) sensor (Table 2.1). The images have a swath of 247.83 km by 249.93 km and a pixel resolution of 30 m. They were visually checked to ensure that the ground was free of ice and snow. These images do not include any clouds or shadows. The Landsat 8 images were already georeferenced in a NAD83 format (UTM Zone 16, Row W) and have eight bands: B1 (0.43–0.45 µm), B2 (0.45–0.51 µm), B3 (0.53–0.59 µm), B4 (0.64–0.67 µm), B5 (0.85–0.88 µm), B6 (1.57– 1.65 µm), B7 (2.11–2.29 µm), and B8 (0.50–0.68 µm). All of them but two were acquired under dry conditions.

Table 2.1. Characteristics of the Landsat-8 OLI images used in this study for Wager Bay North.

Image ID	Date	Time UTC	Cloud cover (%)	Sun elevation (°)	Sun azimuth (°)	Precipitation (mm)(*)
LC80300142013200LGN00	19/07/2013	17h13	15.75	44.84	167.35	33.52
LC80310132013223LGN00	11/08/2013	17h19	0.21	37.99	170.18	0.20
LC80310142013207LGN00	26/07/2013	17h19	0.71	43.40	167.48	0.42
LC80310142013223LGN00	11/08/2013	17h19	2.35	39.23	168.42	0.20
LC80330132013221LGN00	09/08/2013	17h32	1.28	41.04	166.57	0.62
LC80330142013221LGN00	09/08/2013	17h31	0.01	39.81	166.26	0.62
LC80340132014247LGN00	04/09/2014	17h35	0.04	30.03	172.08	16.42
LC80310142014194LGN00	13/07/2014	17h17	0.55	45.83	166.71	6.06
LC80310142015245LGN00	02/09/2015	17h17	17.70	31.95	170.17	1.92
LC80300142015222LGN00	10/08/2015	17h11	1.03	39.47	167.66	0.76

(*) Total of rain equivalent (in mm) during the three days prior to image acquisition, estimated from the mean precipitation recorded at Baker Lake (*64°19′05″N 096°01′03″W)*, Rankin Inlet (62°48′35″N 092°05′58″W), Kugaaruk (68° 32' 0"N, 89° 49' 0"W), Gjoa Haven (68°37′33″N 095°52′30″W), and Hall Beach (68°46′38″N 081°13′27″W)

Nine RADARSAT-2 Scan SAR Wide-A C-band dual-polarized (HH and HV) imagery taken in August of 2014 were also used for this study (Table 2.2). They have a swath of 525.2 km by 266.9 km and a pixel space of 50 m. They were acquired with an incidence angle that varied between 20 and 49.3°. Four SAR images were acquired with the ascending orbit giving an east-look direction and five with the descending orbit giving a west-look direction (Table 2.2). While the ascending orbit images were acquired during dry conditions, the descending orbit images were acquired during dry and wet conditions. Byatt (2014) showed that the accuracy of surficial material maps increases when images acquired over dry and wet conditions are combined. Each imagery file had two images: the HH polarized image and the HV polarized intensity image. All the images were checked visually to ensure the ground was free of snow and ice cover.

Ancillary data used included several 1:50,000 digital elevation model (DEM) tiles (Natural Resources Canada, 2015), which were used for terrain correction when georeferencing the SAR images and for taking into account the topographic effects in the classification. The DEM has a resolution of 16.1 m in the x direction, 23.3 m in the y direction and 1 m in the z direction. Ground elevations are recorded in meter relative to mean sea level (amsl), based on the NAD83 horizontal reference datum. The tiles were downloaded from the GeoGratis database of the Natural Resources Canada website (Natural Resources Canada 2015).

Table 2.2. Characteristics of the RADARSAT-2 dual polarized (C-HH and C-HV) images used in this study for Wager Bay North.

Image ID	Orbit	Date	Local time	Precipitation (mm)	Mosaic ID
RS2_20140808_SCWA_A1 **RS2_20140808_SCWA_A2**	Ascending/East looking direction	8/08/2014	18h21	0.66	A2
RS2_20140825_SCWA_A1 **RS2_20140825_SCWA_A2**	Ascending/ East looking direction	25/08/2014	18h30	0.22	A4
RS2_20140814_SCWA_D1 **RS2_20140814_SCWA_D2**	Descending/West looking direction	14/08/2014	12h19	6.06	D2
RS2_20140824_SCWA_D1 **RS2_20140824_SCWA_D2**	Descending/West looking direction	24/08/2014	12h27	0.18	D4
RS2_20140827_SCWA_D2	Descending/West looking direction	27/08/2014	12h40	0.14	

(*) Total of rain equivalent (in mm) during the three days prior to image acquisition, estimated from the mean precipitation recorded at Baker Lake (*64°19′05″N 096°01′03″W),* Rankin Inlet (62°48′35″N 092°05′58″W), Kugaaruk (68° 32' 0"N, 89° 49' 0"W), Gjoa Haven (68°37′33″N 095°52′30″W), and Hall Beach (68°46′38″N 081°13′27″W)

Two types of GPS sites were used in the study. The first one comprises field observations collected over 346 sites during the summers of 2010, 2011, and 2012 as part of a GEM-1 funded project (McMartin et al., 2015a) They consist of ground pictures, GPS coordinates and descriptions of the surficial deposits and landforms. Each

GPS field site was reclassified into one of the 21 surface material classes as best as possible and verified by the field geologist. However, these GPS field data were mainly collected over till-type surficial deposits, as the main purpose of the GEM-1 funded project was to study and sample the till deposits, but not mapping surface materials at a 30 x 30 m resolution. Thereby, additional 658 sites were located from photo-interpretation of helicopter-based pictures taken as part of the GEM-1 mapping, and Google Earth images. These sites were mainly associated with surficial materials classes other than till. Altogether, the study used 1650 GPS sites. Among them, 650 sites were used to delineate training polygons of at least 10 pixels for a total of 6500 points and about 1000 GPS sites were used to validate the produced map. Both the training and validation GPS sites were all well distributed across the study area (Figure 2.2 a and 2.2 b). Details on the distribution of the training and validation GPS sites among the surficial materials units are given in the *Image classification* section.

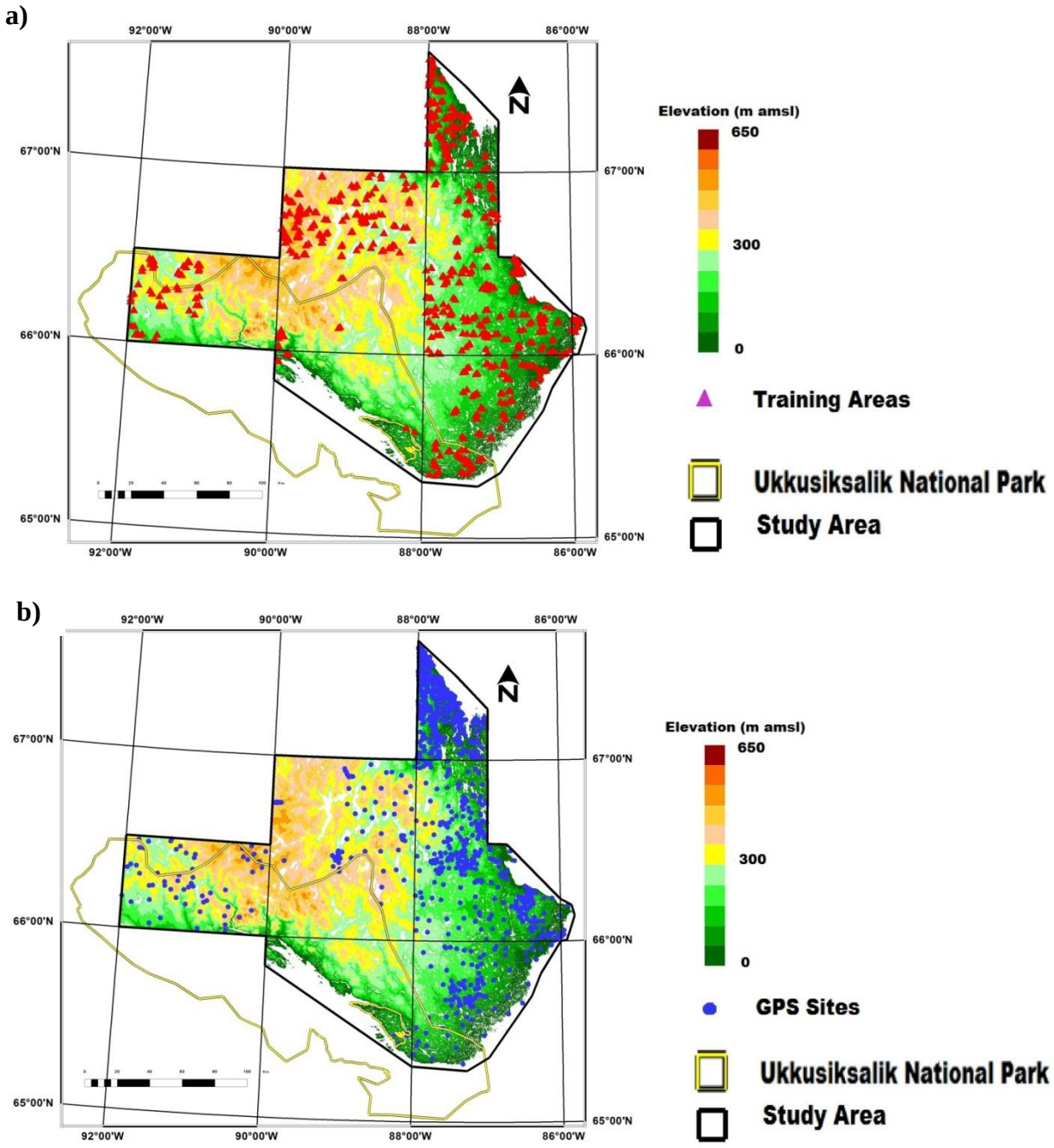

Figure 2.2. Location of a) training areas and b) the GPS validation sites in Wager Bay North.

2.5 METHODS

2.5.1 Image processing

The flowchart of Figure 2.3 presents an overview of the image processing methodology used in the study. The majority of the image processing was performed in *PCI Geomatica* 2015 software. The DEM tiles were first imported and then mosaicked together using the "*Automatic Mosaicking*" menu of the *PCI Geomatica OrthoEngine* module. The parameters used in the mosaicking method were as follows: histogram for the full image, adaptive filter: 20 % of the image, match area: 10 %, cutline: minimum difference, and blend width: 20 pixels. The digital numbers of the Landsat 8 OLI images were first converted into top of atmosphere (TOA) reflectance values, following the method described in the Landsat 8 users handbook (United States Geological Survey, 2015). Such a conversion also removes some of the atmospheric interferences. They were mosaicked together to cover the entire study area with the same *PCI Geomatica* program and related parameters as for the DEM.

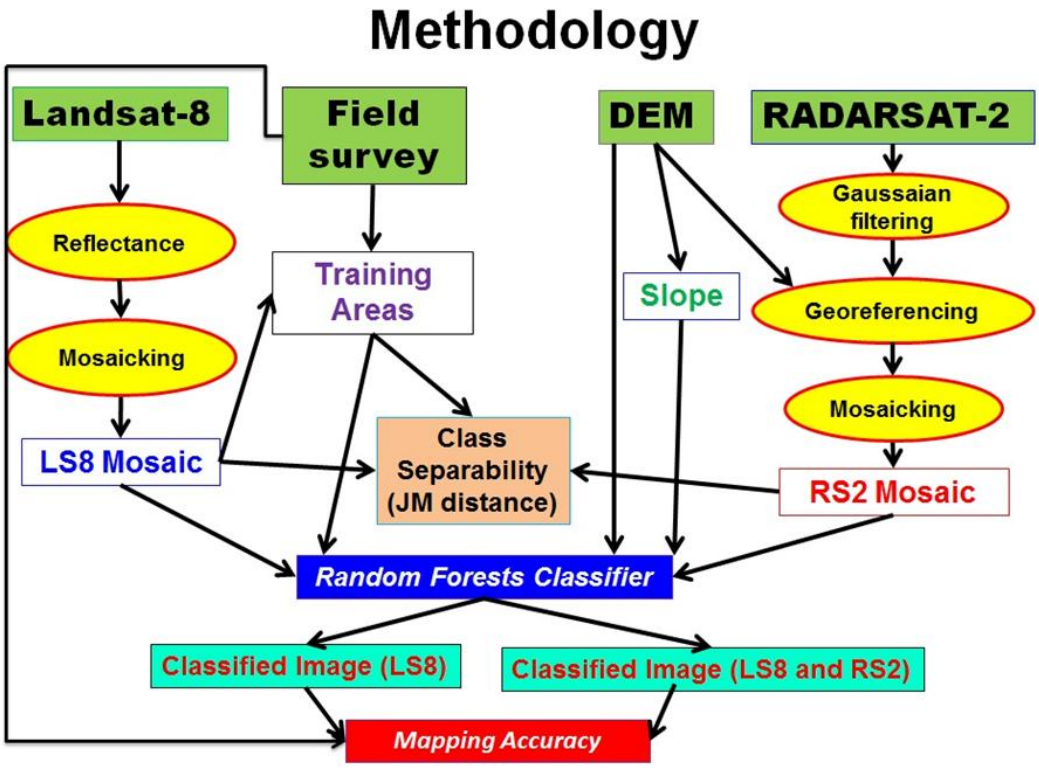

Figure 2.3. Flowchart describing the methodology used in the study.

Following LaRocque et al. (2012), the RADARSAT-2 C-HH and C-HV images were filtered for speckle, using a Gaussian filter (with a standard deviation of 1.6) following the method of Grunsky et al. (2009). Speckle imparts a multiplicative a noise throughout a SAR image and its intensity must be attenuated in order to enhance fine details on SAR images (Goodman, 1976). Each individual image was then orthorectified with the *"RADARSAT-2 Rational Function Model"* function of the *OrthoEngine* module of *PCI Geomatica*, using the DEM and ground control points (GCPs). About 20 GCPs were extracted from the orthorectified Landsat 8 data for georeferencing, which was achieved with a mean accuracy of less than one pixel in both x and y axes (Table 2.3). The

georeferenced images were then mosaicked together to cover the entire study area. This was accomplished using the same *PCI Geomatica* program and related parameters as for the DEM and the Landsat-8 images. The spatial resolution of RADARSAT-2 mosaics were then re-sampled to 30 m to fit with the spatial resolution of the Landsat-8 mosaics using the re-projection menu of *PCI Geomatica Focus* module.

Table 2.3. Orthorectification accuracy (in pixel) of the RADARSAT-2 images used in this study for Wager Bay North.

Image ID	Number of ground control points	RMS error		
		X	Y	Mean
RS2_20140815_SCWA_A1	18	0.77	0.54	0.55
RS2_20140815_SCWA_A2	15	0.84	0.60	0.59
RS2_20140825_SCWA_A1	24	1.09	0.76	0.78
RS2_20140825_SCWA_A2	12	0.78	0.59	0.52
RS2_20140814_SCWA_D1	13	0.82	0.58	0.58
RS2_20140814_SCWA_D2	20	0.70	0.49	0.50
RS2_20140824_SCWA_D1	20	0.75	0.44	0.60

2.5.2 Image classification

Twenty-one surficial material classes were considered in this study. The surficial material classes were defined based on the 12 classes of Campbell et al. (2013), but with some class splitting and combination to better reflect the spectral separability between classes (Table 2.4). In particular, the *Alluvium* (A) class of Campbell et al. (2013) was split into three classes: *alluvial plain (Ap)*, *flooded alluvium (Af),* and *alluvial terrace (At)* to better reflect the variation of moisture levels of each surface material as detailed in Table 2.4. The *bouldery till (bT)* class was split into two classes: *bouldery till (bT)* and *gravelly till (gT)* to better reflect the difference in surface roughness between both materials. The *marine sand (Ms)* class was split in three classes: *marine sand (Ms),*

marine sand with vegetation (MsV), and *thin marine sand (Ms/R)*. *MsV* allows considering the influence of the vegetation cover on the satellite signal, as LaRocque et al. (2012) already showed that considering this factor significantly improves the image classification. *Ms/R* allows for the effect of the material thickness on the satellite signal, which is particularly important for SAR imagery. We merged two *bedrock* classes of Campbell et al. (2013) into a single *bedrock* class *(R),* as there is no difference in surface roughness and satellite signal between both classes. Finally, the marine sediment class called *Mg* in Campbell et al. (2013) was renamed *Mc* to better reflect the silt and clay content in the material. Also the marine sediment class called *M* in Campbell et al. (2013) was renamed *McV* (*Offshore silt and clay with vegetation*) to better reflect the type of material (silt and clay) and the vegetation cover over the surficial material.

Table 2.4. Description of the surficial material classes used in this study for Wager Bay North.

Code	Name	Description
Ap	Alluvial plain	Alluvial sands and minor silts, exposed = periodically water-saturated sediment; alluvial plains, recent deltas and fans; beaches; intertidal flats
Af	Flooded alluvium	Alluvial sediments (sand and silt deposit) periodically covered by small amount of water
At	Alluvial terrace	Exposed sand and minor silt = sandy sediment; mostly dry; alluvial terraces, former deltas and fans
O	Organic	Organics = saturated thin organic sediments; poor drainage; shallow sedge fens and sphagnum bogs
Mc	Offshore silt and clay	Very fine sediments, essentially silt and clay, deposited in the bottom of a quiet water (glaciolacustrine or glaciomarine)
McV	Offshore silt and clay with vegetation	Very fine sediments, essentially silt and clay, deposited in the bottom of a quiet water (glaciolacustrine or glaciomarine), covered by a vegetation growing on the surface
Ms	Marine sand	Sand and minor silt, exposed or lichen-covered = sediments locally wave-washed or winnowed; thick (> 1 m) marine or glaciolacustrine deposits; may include eolian dunes and raised beaches.
MsV	Marine sand with vegetation	Sand and minor silt; covered with short but dense vegetation = sediments locally wave-washed or winnowed; thick (>2 m) marine or glaciolacustrine deposits; may include vegetated eolian dunes and raised beaches.
Ms/R	Thin marine sand	Marine sand and minor silt veneer = sediments locally wave-washed or winnowed; thin (< 1 m) marine or glaciolacustrine deposits; bedrock outcrops may appears but cover less than 50% of the surface.
SG	Sand & Gravel	Sand and gravel, exposed or lichen-covered = proglacial deltas, eskers, outwash terraces, ice-contact glaciofluvial deposits
SGV	Sand & Gravel with vegetation cover	Sand and gravel, covered with short vegetation = proglacial deltas, eskers, outwash terraces, ice-contact glaciofluvial deposits,
T	Thick till	Non-bouldery till = silty-sand to silty–clay diamicton; grass- and lichen-covered; includes blanket and streamlined till; commonly soliflucted; thickness commonly > 1 m
bT	Bouldery till	Bouldery till = silty-sand to sandy diamicton; abundant lichen-covered boulders on surface; includes thin (< 1 m) veneers and thick (> 1 m) deposits of, streamlined till, bouldery till blankets, eroded/modified till and/ or wave-washed (winnowed) till.
cT	Carbonate-rich till	Till with a high degree of carbonate material
gT	Gravelly till	Very coarse till, mainly composed of coarse diamicton, particularly gravel, probably derived from glaciofluvial deposits
gsT	Gravelly sandy till	Coarse till, mainly composed of sand and gravel diamicton.
sT	Sandy till	Sandy till = sandy diamicton, including eroded till; found with undifferentiated glaciofluvial sediments in meltwater corridor complex; thickness commonly between 2 to 5 m; hummock topography interspersed with eroded till features; grass- and/or lichen-covered.
TV	Thick till with dense vegetation cover	Vegetation-covered till = silty-sand to silty–clay diamicton; includes blanket and streamlined till; commonly soliflucted; thickness commonly > 1 m; grass-covered.
T/R	Thin till	Till veneer = silty-sand to sandy diamicton, thin cover interspersed with bedrock outcrops; till thickness commonly < 1 m; bedrock outcrops may appears but cover less than 50% of the surface; may have some boulders; little vegetation.
B	Boulders	Boulders = includes exposed and lichen-covered felsenmeer (broken bedrock) and boulder fields; boulders cover cover more than 50% of the surface; rare discontinuous till and bedrock.
R	Bedrock	Undifferentiated bedrock = intact and frost-riven exposed outcrops of various lithology; bedrock outcrops cover more than 50% of the surface; surface range from rough and weathered to glacially polished and striated, patches of boulders and thin drift cover; may be show lichen-covered outcrop.

Similar to Harris et al. (2008 b), Grunsky et al. (2009), Shelat et al. (2012), and LaRocque et al. (2012), representative training areas of each material class were delineated from air photo-interpretation of the orthorectified Landsat 8 and RADARSAT-2 imagery. Training polygons were delineated within relatively large features, having an area of at least 0.05 km^2, except for *flooded alluvium* (*Af*), where the training areas only covered 0.036 km^2, because this unit is relatively small in the region (Table 2.5).

Table 2.5. Training area polygon characteristics and GPS validation sites.

Class	Number of training polygons	Number of pixels	Area (km^2)	Percent of image (%)	Number of GPS validation sites
Ap	20	200	0.180	0.000696	28
Af	4	40	0.036	0.000139	5
At	14	140	0.126	0.000487	27
O	22	220	0.198	0.000766	17
Mc	22	220	0.198	0.000766	30
McV	22	220	0.198	0.000766	83
Ms	12	120	0.108	0.000418	26
MsV	8	80	0.072	0.000279	46
Ms/R	34	340	0.306	0.001184	43
SG	38	380	0.342	0.001323	67
SGV	30	300	0.270	0.001045	31
T	54	540	0.486	0.001880	98
bT	66	660	0.594	0.002298	126
cT	16	160	0.144	0.000557	24
gT	10	100	0.090	0.000348	20
gsT	12	120	0.108	0.000418	32
sT	10	100	0.090	0.000348	23
TV	6	60	0.054	0.000209	13
T/R	134	1340	1.206	0.004666	171
B	38	380	0.342	0.001323	47
R	78	780	0.702	0.002716	47
Total	**650**	**6500**	**5.85**	**0.022633**	**1004**

The training areas were then used to compute class spectral signatures. Landsat-8 OLI data measure the reflective properties of the surficial materials in the visible, near-infrared, and shortwave-infrared wavelengths of the electromagnetic spectrum. These reflective properties are highly related to the presence or absence of vegetation that has a strong reflectance in green (B3) and near-infrared (B5) bands. They are also related to moisture content of surficial materials. The RADARSAT-2 images are related to the backscatter properties in each polarization (HH, HV) of the surficial materials, which depend on surface roughness, morphology (geometry), and moisture content.

The accuracy of image classification greatly depends on the spectral separability between classes. In this study, the spectral separability was assessed by the Jeffries-Matusita (J-M) distance, which has values ranging from 0 to 2. A value between 0 and 1 indicates a very poor separation, 1 and 1.9 suggests a moderate separation, and 1.9 and 2.0 reflects a good separation (Richards, 1993).

The classifier used in this study is a non-parametric decision-tree–type classifier (RF), which does not assume normal distribution of the input data (Breiman, 2001, 2003). The algorithm used for this study was developed in R programming language (R Development Core Team, 2012), which has recently been successfully employed in a study on surficial material mapping in the Hudson Bay Lowlands (Ou et al., 2016). The RF classifier has two versions, known as "*all-polygon*" and "*sub-polygon*". The *all-polygon* version uses all of the pixels within all of the training area polygons to define class training areas, whereas the *sub-polygon* version randomly selects a user-determined number of training area pixels from each class. While the *all-polygon* version has the advantage of taking into account the actual class size, we also used the

sub-polygon version that has the advantage of reducing the risk of spatial autocorrelation in the analysis. The settings of the classifier were a forest of 500 independent decision trees with the default values for the *mtry* variable. The *mtry* variable in Random Forests refers to the number of variables randomly sampled as candidates at each split of every node. The default values of *mtry* for a classification are calculated as the square root of *p*, where *p* is the number of variables in the matrix of predictors for the classification (*x*). Such default values lead to a setting that includes all input features, that is, all pixels are randomly sampled as candidates at each split of every node.

The RF classifier uses two-thirds of the input training-area data, referred to as *in-bag* data, for calibration. The remaining third of the data is then referred to as *out-of-bag* data and is used to test or validate the resulting classification. *In-bag* data are used to create the 500 individual decision trees, which are applied to produce independent classifications. These independent classifications are then combined into the final classification map (Waske and Braun, 2009). When there are relatively limited training data in some classes, the RF classifier allows bootstrap aggregating of the *in-bag* data to increase the number of training pixels. In this study, each class of the study area had enough training sites, so bootstrapping was not required.

The RF classifier is not sensitive to noise. Another advantage of the RF classifier is that it outperforms the widely-used maximum likelihood classifier (MLC). For the same combination of input data, the RF classifier consistently gives a better overall accuracy than MLC, as shown in several land-cover mapping studies (Waske and Braun, 2009; Ozdarici-Ok et al., 2012; LaRocque et al., 2013; LaRocque et al. 2014). Additionally, it can handle a higher number of input data (optical, SAR, DEM), regardless of their data

distribution, whereas MLC mainly handles Gaussian-distributed data. Finally, RF can estimate the importance of the individual input variables (Gislason et al., 2006; Waske and Braun, 2009). Indeed, the RF classifier produces a variable importance plot that ranks the classifier input data as a function of their degree of usefulness in the classification. The higher the input data is on the Y axis of the variable importance plot, the more useful the data is in performing the classification (Strobl et al., 2008; Louppe et al., 2013).

For both the J-M distance computation and the classifier, three image combinations were considered: 1) only the Landsat-8 OLI images; 2) only the RADARSAT-2 images, and 3) a combination of Landsat-8 OLI and RADARSAT-2 images. In each case, DEM and slope were added to the classification to take into account topographic (elevation) information of each class. Also, the classifier was applied to the images where background, lakes, rivers, and other water bodies were masked out with a mask that was created from a combination of Landsat 8 B8 and RADARSAT-2 C-HV images.

2.5.3 Accuracy assessment

Classification accuracy was assessed first by comparing training areas with the equivalent classified land use in the imagery. Such comparison was performed under the form of a "confusion matrix" or error matrix", where each cell expresses the number of pixels classified to a particular class in relation to the class defined by the training areas (Congalton 1991). The confusion matrix allows computing individual user's and producer's class accuracies and their related errors (omission and commission), as described in Congalton (1991). The User's class accuracy corresponds to the probability

that a pixel of the classified image is in the correct class, the associated number of misclassified pixels being pixels classified in the incorrect class (error of omission). The Producer's accuracy measures the probability that a reference pixel is effectively well classified, the associated number of misclassified pixels being pixels that actually belong to another class (error of commission).

From the confusion matrix, it is also possible to compute the average and overall accuracies. The average accuracy was computed as the simple average between User's class accuracies, whereas the overall accuracy is the average of individual class User's or Producer's accuracies, weighted by the size of the class in the classified or reference image.

The best classified image was selected, based on the highest overall accuracy and the visual evaluation of each classified image produced. However, such a method only gives an assessment of the classified image accuracy that is different than the true mapping accuracy. A more robust and independent accuracy assessment is to compare the resulting classified image with an independent set of GPS field observation data acquired over the validation sites. If the image returns the same class as the one observed at the validation site, then the pixel related to this validation site is associated to a value of 1. If it is not the case, then the value is zero. A confusion matrix between the ground truth and classified image can then be computed.

2.6 RESULTS AND DISCUSSION

2.6.1 J-M Distance

J-M distances were computed for both the Landsat-8 TIM images alone (Table 2.6) or with RADARSAT-2 SAR images (Table 2.7). The Landsat-8 images showed a generally good separability for the majority of the surficial classes, with most J-M distances being above 1.9. The average J-M distance was 1.961, with a minimum value of 1.172 between *sandy till (sT)* and *thin till over bedrock (T/R)*. There were 19 other class pairs that have a J-M distance lower than 1.85, indicating some confusion between these classes. Despite the higher number of classes considered here, our minimum and average J-M distances with Landsat-8 images were higher than those of Shelat et al (2012), LaRocque et al. (2012), and Campbell et al (2013). These studies used Landsat-7 ETM+ images which have a lower spectral resolution than Landsat-8 images, because Landsat-7 ETM+ images have less bands and larger band widths than Landsat-8 images. Another reason might also be that our delineated training areas are of better quality that the ones used in these studies. Also, our study included data from both wet and dry surface conditions which can help to distinguish some surficial classes from each other due to the nature of the material, as already shown in Byatt (2014).

Table 2.6. J-M distances computed for the Landsat-8 OLI images used in this study.

Class	Ap	Af	At	O	Mc	McV	Ms	MsV	Ms/R	SG	SGV	T	bT	cT	gT	gsT	sT	TV	T/R	B
Af	2.000																			
At	2.000	2.000																		
O	1.996	2.000	1.648																	
Mc	2.000	2.000	1.406	1.841																
McV	2.000	2.000	2.000	2.000	2.000															
Ms	1.997	2.000	1.645	1.563	1.555	2.000														
MsV	2.000	2.000	2.000	2.000	2.000	2.000	2.000													
Ms/R	2.000	2.000	2.000	2.000	2.000	2.000	2.000	2.000												
SG	2.000	2.000	2.000	2.000	2.000	2.000	1.998	2.000	2.000											
SGV	2.000	2.000	2.000	2.000	2.000	2.000	2.000	2.000	2.000	2.000										
T	2.000	2.000	1.998	1.981	2.000	2.000	1.997	1.998	2.000	2.000	1.999									
bT	2.000	2.000	1.993	1.956	1.998	2.000	1.990	2.000	2.000	2.000	1.998	1.933								
cT	2.000	2.000	1.947	1.835	1.976	2.000	1.927	2.000	2.000	2.000	2.000	1.964	1.892							
gT	2.000	2.000	1.965	1.949	2.000	2.000	1.947	2.000	1.999	1.999	1.997	1.951	1.939	1.941						
gsT	2.000	2.000	1.984	1.905	1.999	2.000	1.971	1.999	1.999	2.000	1.998	1.735	1.916	1.893	1.651					
sT	2.000	2.000	1.998	1.989	2.000	2.000	1.996	2.000	1.995	2.000	1.997	1.704	1.949	1.973	1.895	1.796				
TV	2.000	2.000	2.000	2.000	2.000	2.000	2.000	2.000	2.000	2.000	2.000	1.999	2.000	2.000	2.000	2.000	2.000			
T/R	2.000	2.000	1.997	1.985	2.000	2.000	1.995	2.000	1.994	2.000	1.994	1.763	1.903	1.944	1.782	1.721	1.172	2.000		
B	2.000	2.000	1.998	1.986	2.000	2.000	1.995	2.000	2.000	2.000	1.998	1.804	1.978	1.987	1.925	1.802	1.512	2.000	1.553	
R	2.000	2.000	2.000	2.000	2.000	2.000	2.000	2.000	2.000	2.000	2.000	2.000	2.000	2.000	2.000	2.000	2.000	2.000	1.999	1.999

J-M distance: Minimum= 1.172; Mean = 1.961; Maximum=2.000

Table 2.7. J-M distances computed for the Landsat-8 and RADARSAT-2 dual-pol (HH, HV) images used in this study.

Class	Ap	Af	At	O	Mc	McV	Ms	MsV	Ms/R	SG	SGV	T	bT	cT	gT	gsT	sT	TV	T/R	B
Af	2.000																			
At	2.000	2.000																		
O	2.000	2.000	1.943																	
Mc	2.000	2.000	1.892	1.956																
McV	2.000	2.000	2.000	2.000	2.000															
Ms	2.000	2.000	1.896	1.905	1.903	2.000														
MsV	2.000	2.000	2.000	2.000	2.000	2.000	2.000													
Ms/R	2.000	2.000	2.000	2.000	2.000	2.000	2.000	2.000												
SG	2.000	2.000	2.000	2.000	2.000	2.000	2.000	2.000	2.000											
SGV	2.000	2.000	2.000	2.000	2.000	2.000	2.000	2.000	2.000	2.000										
T	2.000	2.000	2.000	1.998	2.000	2.000	2.000	2.000	2.000	2.000	2.000									
bT	2.000	2.000	2.000	1.997	2.000	2.000	1.999	2.000	2.000	2.000	1.999	1.983								
cT	2.000	2.000	2.000	2.000	2.000	2.000	1.999	2.000	2.000	2.000	2.000	1.999	1.999							
gT	2.000	2.000	2.000	1.999	2.000	2.000	1.998	2.000	2.000	2.000	2.000	1.999	1.997	2.000						
gsT	2.000	2.000	2.000	1.990	2.000	2.000	1.999	2.000	2.000	2.000	2.000	1.965	1.988	2.000	1.992					
sT	2.000	2.000	2.000	2.000	2.000	2.000	2.000	2.000	1.999	2.000	2.000	1.966	1.999	2.000	2.000	2.000				
TV	2.000	2.000	2.000	2.000	2.000	2.000	2.000	2.000	2.000	2.000	2.000	2.000	2.000	2.000	2.000	2.000	2.000			
T/R	2.000	2.000	2.000	1.999	2.000	2.000	2.000	2.000	1.997	2.000	1.999	1.908	1.975	1.997	1.994	1.960	1.898	2.000		
B	2.000	2.000	2.000	1.999	2.000	2.000	2.000	2.000	2.000	2.000	2.000	1.984	1.996	2.000	1.999	1.991	1.996	2.000	1.857	
R	2.000	2.000	2.000	2.000	2.000	2.000	2.000	2.000	2.000	2.000	2.000	2.000	2.000	2.000	2.000	2.000	2.000	2.000	2.000	2.000

J-M distance: Minimum= 1.857; Mean = 1.995; Maximum=2.000

The J-M distance computed for the combination of Landsat-8 and RADARSAT-2 SAR images showed a much better separability of the surface material classes. The mean J-M distance was 1.995 and the minimum was 1.857, which corresponds to the separability between *thin till over bedrock (T/R)* and *boulders (B)*. The other three J-M distances lower than 1.9 but higher than 1.85 corresponded to the following class pairs: *Alluvial terrace (At)* with *marine clay (Mc)* (1.892) or *marine sand (Ms)* (1.896) as well as *thin till over bedrock (T/R)* with *sandy till (sT)* (1.898). *Alluvial terrace (At), marine clay (Mc),* and *marine sand (Ms)* are all dry and well-exposed (no vegetation) surficial materials, and may contain material with similar grain sizes that may naturally grade into each other. *Thin till over bedrock (T/R)* and *sandy till (sT)* have similar coarse grain sizes (sand) than *thick till (TV)* because both first classes are more locally-derived.

2.6.2 Classification accuracies

When only Landsat-8 data are used as image data, the classification overall accuracy is 90.6% for the *Sub-polygon* script and 92.8% with the *All-polygon* script (Table 2.8). These accuracies are higher than those obtained by Grunsky et al. (2009) (84.8%), Shelat et al. (2012) (80.3%), LaRocque et al. (2012) (86.2%), and Campbell et al. (2013) (46.3%). All these studies used the low spectral resolution Landsat-7 ETM+ images and the maximum likelihood classifier, which was shown to be less efficient than Random Forests in several land use classification studies (Waske and Braun, 2009; Ozdarici-Ok et al., 2012; LaRocque et al., 2013). In addition DEM and slope data were also added to the classification and both ranked very highly in the variable importance plot (Figure 2.4).

Table 2.8. Class accuracies (in %) obtained by applying the Random Forests classifier (Sub- and All-Polygon versions) to a combination of DEM, slope, and image data as a function of the images used in the classification.

Class	Sub-Polygon				All-Polygon			
	User's accuracy		Producer's accuracy		User's accuracy		Producer's accuracy	
	Landsat-8	Landsat-8 & Radarsat-2	Landsat-8	Landsat-8 & Radarsat-2	Landsat-8	Landsat-8 & Radarsat-2	Landsat-8	Landsat-8 & Radarsat-2
Ap	97.1	99.0	98.1	100	99.5	99.0	98.5	100
Af	81.8	100	90.0	100	95.0	100	100	100
At	84.4	99.0	89.0	99.0	75.0	100	88.9	100
O	88.2	91.0	94.3	100	94.5	99.4	98.3	99.4
Mc	95.9	95.9	77.0	98.3	95.0	99.6	74.5	98.8
McV	98.3	100	95.9	97.5	98.6	99.5	96.9	98.6
Ms	97.1	100	97.1	97.2	98.6	100	98.6	97.9
MsV	97.7	97.7	97.7	97.7	97.5	100	100	98.8
Ms/R	87.5	94.0	91.6	97.4	93.0	99.0	93.9	99.0
SG	67.3	90.8	89.6	96.9	76.7	95.7	92.2	99.0
SGV	71.5	83.3	88.7	92.5	74.9	91.4	93.7	97.6
T	94.7	97.9	90.8	96.8	97.2	99.1	94.8	98.4
bT	95.6	99.4	90.8	97.3	96.8	99.0	95.0	98.1
cT	87.5	98.9	92.8	100	96.3	98.8	95.1	100
gT	64.3	89.1	83.7	92.5	68.0	90.0	91.9	95.7
gsT	96.6	98.3	95.0	96.7	98.6	98.6	99.3	100
sT	80.6	86.6	98.2	98.3	81.0	89.0	95.3	97.8
TV	85.3	97.1	96.7	97.1	96.7	100	90.6	100
T/R	96.1	98.9	89.5	94.6	96.6	99.0	91.6	97.2
B	95.6	96.1	96.5	99.5	95.6	98.0	97.8	99.3
R	92.0	97.5	87.2	94.0	93.5	98.0	89.5	96.3
Average	**88.3**	**95.7**	**91.9**	**97.3**	**91.4**	**97.8**	**94.1**	**98.7**
Overall	**90.6**	**96.4**	**90.6**	**96.4**	**92.8**	**98.1**	**92.8**	**98.1**

Adding RADARSAT-2 in the classification greatly improves the classification overall accuracies which increase from 90.6% to 96.4% in the case of the sub-polygon script and from 92.8% to 98.1% in the case of the all-polygon script. This finding is consistent with those of Grunsky et al. (2009), Shelat et al. (2012), and LaRocque et al. (2012) who showed that adding SAR images in the classifier improves the classification overall accuracy for surficial materials mapping in the Arctic. With respect to the Landsat-8 we achieved higher accuracies than those obtained by Grunsky et al. (2009) (91.9%), Shelat et al. (2012) (84.0%), and LaRocque et al. (2012) (93.2%). The combination of Landsat-

8 and RADARSAT-2 results in the highest classification accuracies, and as such we will only present and discuss this case for the remaining of the study. As shown in Figure 2.4, for both the *sub-polygon* and *all-polygon* scripts, RADARSAT-2 descending orbit images acquired under dry conditions (mosaic#D4) have higher importance in the classification than those acquired under wet conditions (mosaic#D2).The descending SAR images also have a higher importance than the Landsat-8 B3 (green) and B4 (red) images. For the *all-polygon* script, the HV images are generally better predictors than the HH image, confirming the role of HV images for surficial material mapping already showed in Shelat et al. (2012) and LaRocque et al. (2012).

The resulting surficial material maps produced by applying the Random Forests classifier applied to a combination of Landsat-8, RADARSAT-2 HH / HV, DEM and slope data is presented in Figure 2.5 for the *sub-polygon* script and in Figure 2.6 for the *all-polygon* script. Figure 2.7 compares the distribution of the surficial material areas as extracted from the surficial material maps produced by the *sub-polygon* script and the *all-polygon* script. Both scripts gave a similar areal distribution of each surficial material unit.

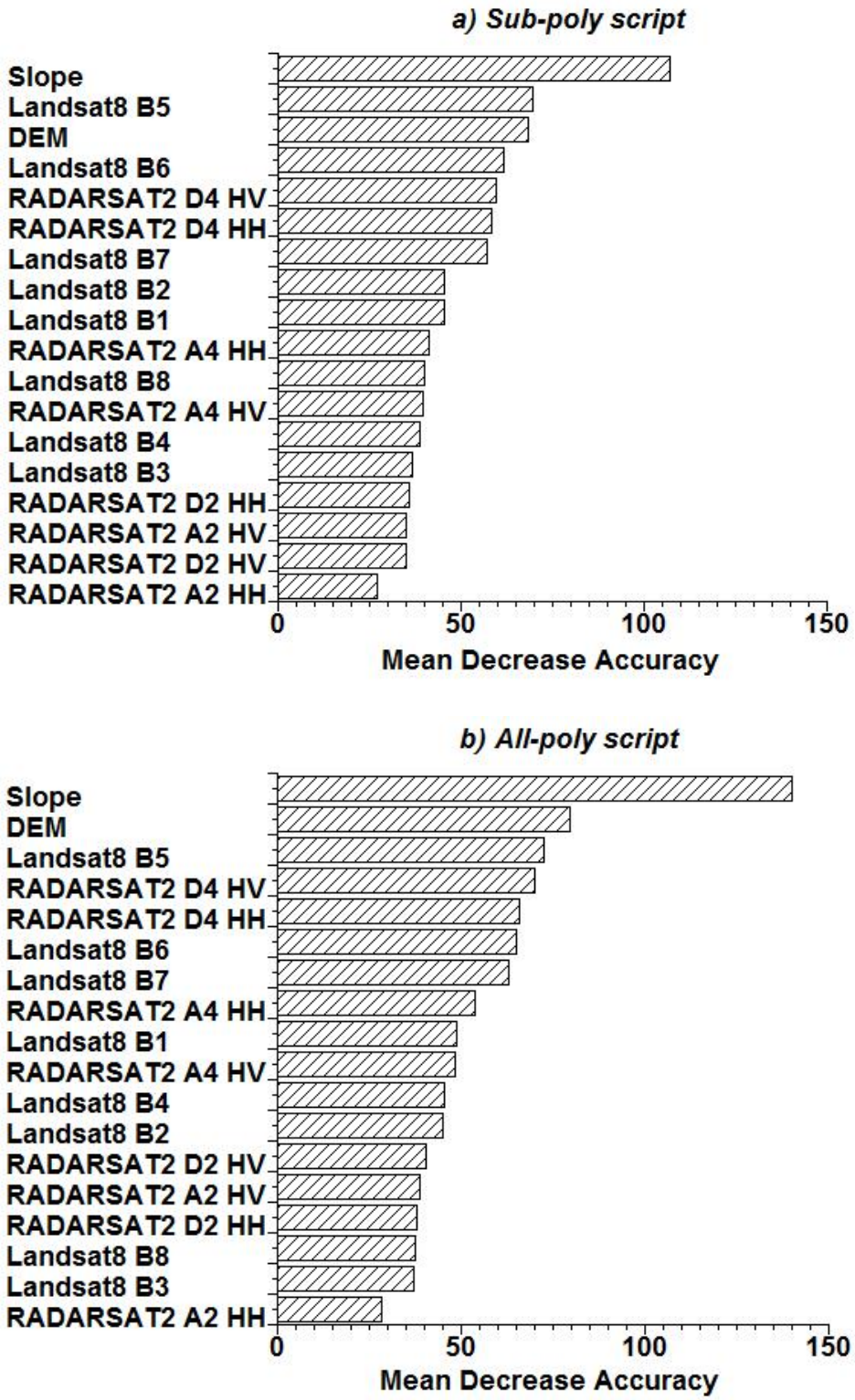

Figure 2.4. Variable importance plots with the Random Forest classifier applied to a combination of Landsat-8, RADARSAT-2 HH / HV, DEM and slope data for a) the sub-polygon script and b) the all-polygon scrip.

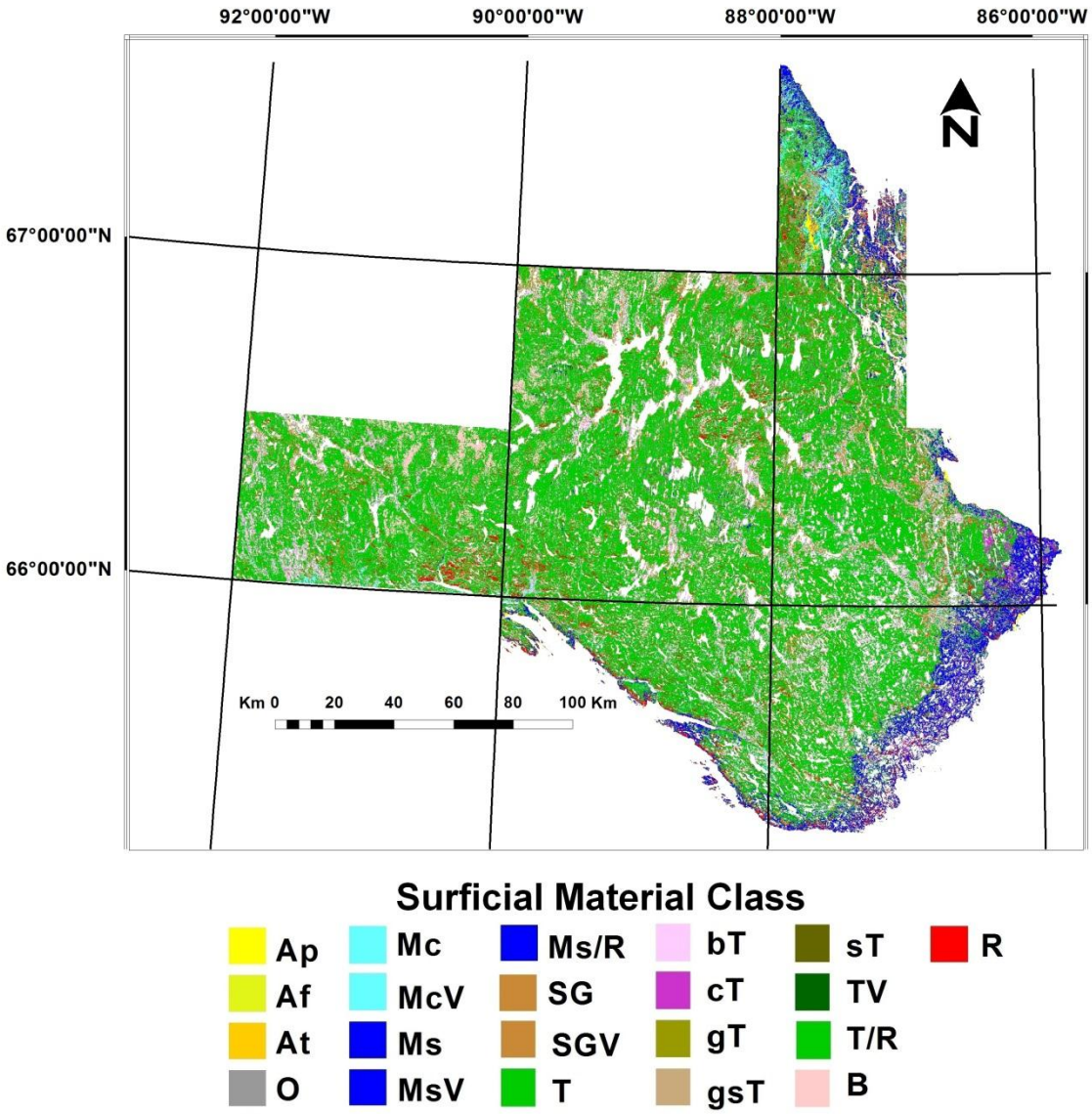

Figure 2.5. Surficial material map for the northern Wager Bay area produced by a Random Forest classifier applied to a combination of Landsat-8, RADARSAT-2 HH / HV, DEM and slope data using the Sub-polygon script.

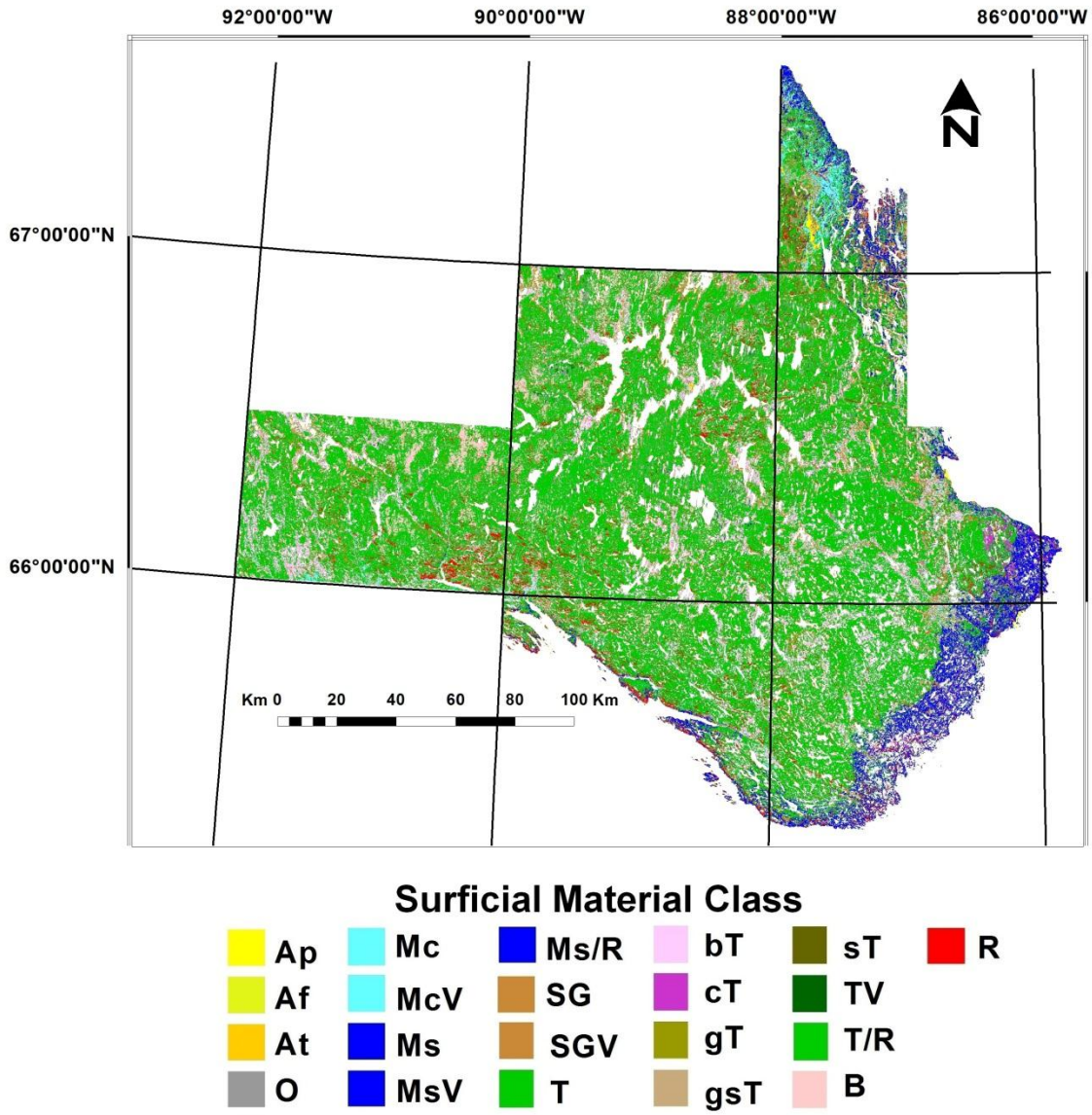

Figure 2.6. Surficial material map for the northern Wager Bay area produced by a Random Forest classifier applied to a combination of Landsat-8, RADARSAT-2 HH / HV, DEM and slope data using the All-polygon script.

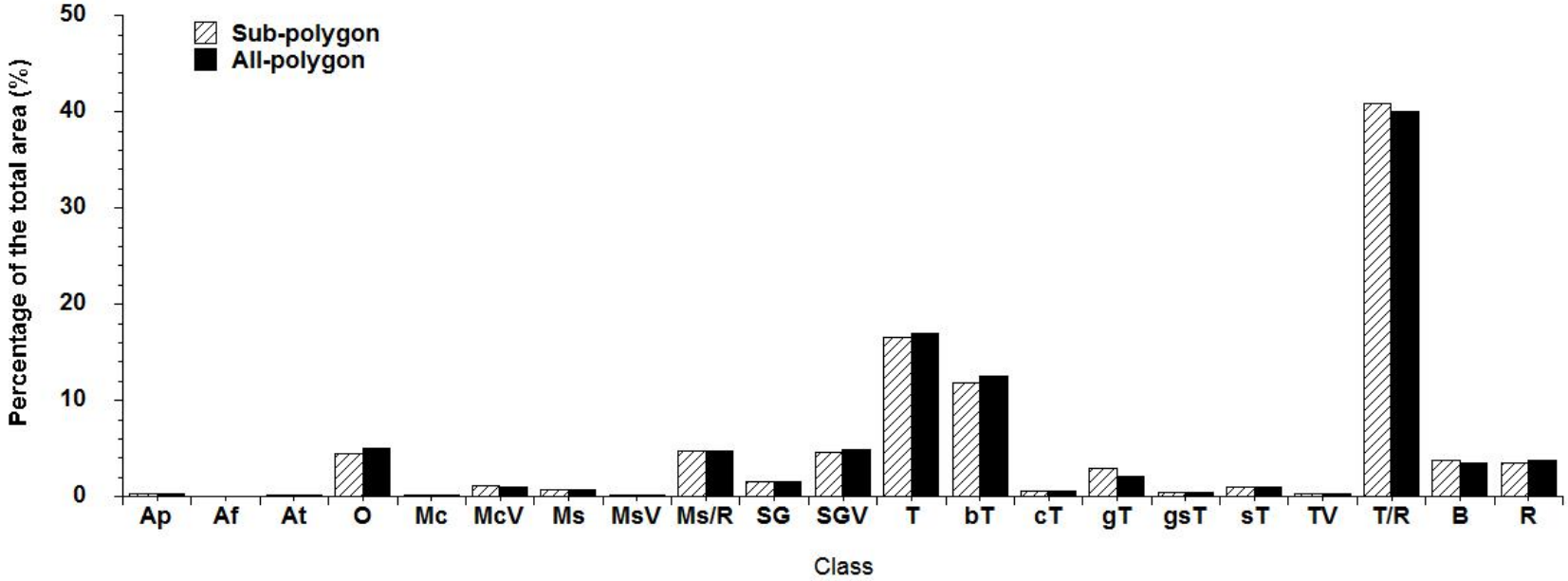

Figure 2.7. Distribution of the surficial material areas as extracted from the surficial material maps produced by the sub-polygon script and the all-polygon script.

The confusion matrices related to the classification are shown in Table 2.9 for the *sub-polygon* script and in Table 2.10 for the *all-polygon* script. With the *sub-polygon* script, all the classes have a user's and producer's class accuracy above 95%, except six classes in the case of the user's class accuracy and four classes in the case of the producer's class accuracy. The *sand and gravel with vegetation (SGV)* class has the highest error of omission (16.7%), mainly because of a confusion with the *thin till over bedrock* (*T/R)* class. Other classes showing high errors of omission are *sandy till (sT)* (13.4%) and *gravelly till (gT)* (10.9%). For *sT*, the confusion mainly occurs with the *thin till over bedrock (T/R)* class and with the *bedrock (R)* class. For *gT*, the confusion mainly occurs with *sand and gravel with vegetation (SGV)*, *thick till (T)*, and *bouldery till (bT)*. The three other classes that are associated to errors of omission higher than 5% are: *thin marine sand (Ms/R)* (6%), *organic (O)* (9.0%) and *sand and gravel (SG)* (9.2%). *Ms/R* is mainly confused with the *bedrock (R)* class. *O* is mainly confused with *offshore silt and clay with vegetation (McV), thick till (T),* and *thin till over bedrock* (*T/R)*. *SG* has confusion with *sand and gravel with vegetation (SGV), thin till over bedrock* (*T/R),* and *bedrock (R)*. The *sand and gravel with vegetation (SGV)* class and *gravelly till (gT)* have both the highest error of commission (7.5%), because of a confusion with the *sand and gravel (SG)* class for the first and with the *sand and gravel with vegetation (SGV)* for the second. The two other classes that are associated to errors of commission higher than 5% are: *thin till over bedrock* (*T/R)* (5.4%) and *bedrock (R)* (6.0%). *T/R* is mainly confused with *sand and gravel with vegetation (SGV), boulders (B)* and *bedrock (R). Bedrock (R)* is mainly confused with *thin marine sand (Ms/R).*

Table 2.9. Confusion matrix (in number of pixels) when the Random Forests Sub-Polygon classifier is applied to the combination of Landsat-8 OLI, RADARSAT-2, DEM, and slope data.

Class	Ap	Af	At	O	Mc	McV	Ms	MsV	Ms/R	SG	SGV	T	bT	cT	gT	gsT	sT	TV	T/R	B	R	User's Accuracy	Error of Omission
Ap	**98**	0	0	0	0	0	1	0	0	0	0	0	0	0	0	0	0	0	0	0	0	99.0	1.0
Af	0	**11**	0	0	0	0	0	0	0	0	0	0	0	0	0	0	0	0	0	0	0	100	0.0
At	0	0	**95**	0	0	0	0	0	0	1	0	0	0	0	0	0	0	0	0	0	0	99.0	1.0
O	0	0	0	**81**	0	2	0	0	0	0	0	2	0	0	0	1	0	1	2	0	0	91.0	9.0
Mc	0	0	0	0	**118**	0	0	0	0	4	0	0	0	0	0	0	0	0	0	0	1	95.9	4.1
McV	0	0	0	0	0	**119**	0	0	0	0	0	0	0	0	0	0	0	0	0	0	0	100	0.0
Ms	0	0	0	0	0	0	**70**	0	0	0	0	0	0	0	0	0	0	0	0	0	0	100	0.0
MsV	0	0	0	0	0	0	0	**43**	0	0	0	1	0	0	0	0	0	0	0	0	0	97.7	2.3
Ms/R	0	0	0	0	0	0	0	0	**188**	0	1	0	0	0	0	0	0	0	1	0	10	94.0	6.0
SG	0	0	1	0	0	0	0	0	0	**187**	5	1	3	0	0	1	0	0	4	0	4	90.8	9.2
SGV	0	0	0	0	0	0	0	1	4	1	**135**	2	0	0	2	0	0	0	15	0	2	83.3	16.7
T	0	0	0	0	0	1	0	0	0	0	0	**276**	4	0	1	0	0	0	0	0	0	97.9	2.1
bT	0	0	0	0	0	0	0	0	0	0	0	0	**358**	0	1	0	0	0	1	0	0	99.4	0.6
cT	0	0	0	0	0	0	0	0	0	0	0	0	1	**87**	0	0	0	0	0	0	0	98.9	1.1
gT	0	0	0	0	0	0	0	0	0	0	2	2	2	0	**49**	0	0	0	0	0	0	89.1	10.9
gsT	0	0	0	0	0	0	0	0	0	0	0	0	0	0	0	**58**	1	0	0	0	0	98.3	1.7
sT	0	0	0	0	0	0	1	0	0	0	1	0	0	0	0	0	**58**	0	4	0	3	86.6	13.4
TV	0	0	0	0	0	0	0	0	0	0	0	1	0	0	0	0	0	**33**	0	0	0	97.1	2.9
T/R	0	0	0	0	0	0	0	0	1	0	1	0	0	0	0	0	0	0	**730**	1	5	98.9	1.1
B	0	0	0	0	0	0	0	0	0	0	0	0	0	0	0	0	0	0	8	**195**	0	96.1	3.9
R	0	0	0	0	2	0	0	0	0	0	1	0	0	0	0	0	0	0	**7**	0	**393**	97.5	2.5
Producer's Accuracy	100	100	99.0	100	98.3	97.5	97.2	97.7	97.4	96.9	92.5	96.8	97.3	100	92.5	96.7	98.3	97.1	94.6	99.5	94.0		
Error of Commission	0.0	0.0	1.0	0.0	1.7	2.5	2.8	2.3	2.6	3.1	7.5	3.2	2.7	0.0	7.5	3.3	1.7	2.9	5.4	0.5	6.0		

Table 2.10. Confusion matrix (in number of pixels) when the Random Forests All-Polygon classifier is applied to the combination of Landsat-8 OLI, RADARSAT-2, DEM, and slope data.

Class	Ap	Af	At	O	Mc	McV	Ms	MsV	Ms/R	SG	SGV	T	bT	cT	gT	gsT	sT	TV	T/R	B	R	User's Accuracy	Error of Omission
Ap	**193**	0	0	0	0	0	2	0	0	0	0	0	0	0	0	0	0	0	0	0	0	99.0	1.0
Af	0	**20**	0	0	0	0	0	0	0	0	0	0	0	0	0	0	0	0	0	0	0	100	0.0
At	0	0	**160**	0	0	0	0	0	0	0	0	0	0	0	0	0	0	0	0	0	0	100	0.0
O	0	0	0	**174**	0	1	0	0	0	0	0	0	0	0	0	0	0	0	0	0	0	99.4	0.6
Mc	0	0	0	0	**239**	0	0	0	0	1	0	0	0	0	0	0	0	0	0	0	0	99.6	0.4
McV	0	0	0	0	0	**219**	0	0	0	0	0	1	0	0	0	0	0	0	0	0	0	99.5	0.5
Ms	0	0	0	0	0	0	**140**	0	0	0	0	0	0	0	0	0	0	0	0	0	0	100	0.0
MsV	0	0	0	0	0	0	0	**80**	0	0	0	0	0	0	0	0	0	0	0	0	0	100	0.0
Ms/R	0	0	0	0	0	0	0	0	**396**	1	0	0	0	0	0	0	0	0	0	0	3	99.0	1.0
SG	0	0	0	0	2	0	1	0	0	**382**	4	0	3	0	0	0	0	0	2	0	5	95.7	4.3
SGV	0	0	0	0	0	0	0	1	2	2	**288**	1	0	0	2	0	0	0	15	0	4	91.4	8.6
T	0	0	0	1	0	1	0	0	1	0	0	**557**	2	0	0	0	0	0	0	0	0	99.1	0.9
bT	0	0	0	0	0	0	0	0	0	0	0	3	**713**	0	2	0	0	0	2	0	0	99.0	1.0
cT	0	0	0	0	0	0	0	0	0	0	0	1	1	**158**	0	0	0	0	0	0	0	98.8	1.3
gT	0	0	0	0	0	0	0	0	0	0	0	1	8	0	**90**	0	0	0	1	0	0	90.0	10.0
gsT	0	0	0	0	0	1	0	0	0	0	0	0	0	0	0	**139**	1	0	0	0	0	98.6	1.4
sT	0	0	0	0	0	0	0	0	0	0	1	2	0	0	0	0	**89**	0	2	0	6	89.0	11.0
TV	0	0	0	0	0	0	0	0	0	0	0	0	0	0	0	0	0	**60**	0	0	0	100	0.0
T/R	0	0	0	0	0	0	0	0	0	0	2	0	0	0	0	0	0	0	**1446**	3	10	99.0	1.0
B	0	0	0	0	0	0	0	0	0	0	0	0	0	0	0	0	0	0	6	**401**	2	98.0	2.0
R	0	0	0	0	1	0	0	0	1	0	0	0	0	0	0	0	1	0	13	0	**783**	98.0	2.0
Producer's Accuracy	100	100	100	99.4	98.8	98.6	97.9	98.8	99.0	99.0	97.6	98.4	98.1	100	95.7	100	97.8	100	97.2	99.3	96.3		
Error of Commission	0.0	0.0	0.0	0.6	1.2	1.4	2.1	1.2	1.0	1.0	2.4	1.6	1.9	0.0	4.3	0.0	2.2	0.0	2.8	0.7	3.7		

With the *all-polygon* script, all the classes have a user's and producer's class accuracy higher than with the *sub-polygon* script, except for the user's class accuracy in the case of *marine sand (Ms)* and the producer's class accuracy in the case of *organic (O).* All the user's and producer's class accuracies are above 98%, except four classes in the case of the user's class accuracy and six classes in the case of the producer's class accuracy. There are two classes that have the highest errors of omission: *sandy till (sT)* (11.0%), mainly because of confusion with *bedrock (R),* and *gravelly till (gT)* (10.0%), mainly because of confusion with *bouldery till (bT).* The other classes which have high error of omission are *sand and gravel with vegetation (SGV)* (8.6%) because of a confusion with *thin till over bedrock* (*T/R)* and *sand and gravel (SG)* (4.3%) because of a confusion with *bedrock (R)* and *sand and gravel with vegetation (SGV).* The highest error of commission (4.3%) occurs for *gravelly till (gT)* because of confusion with *sand and gravel with vegetation (SGV)* and with *bouldery till (bT).* The *bedrock (R)* class has an error of commission of 3.7% mainly because of confusion with *thin till over bedrock* (*T/R).* Four classes have an error of commission between 2 and 3%: *thin till over bedrock* (*T/R)* (2.8%) because of confusion with *bedrock (R), sand and gravel with vegetation (SGV)* (2.4%) because of confusion with *sand and gravel (SG), sandy till (sT)* because of confusion with *bedrock (R)* and *gravelly sandy till (gsT),* and *marine sand (Ms)* because of confusion with *alluvial plain (Ap).*

Whatever the script, all the user's class and producer's class accuracies are higher than those published by Grunsky et al. (2009), Shelat et al. (2012), and LaRocque et al. (2012). Despite these high class accuracies, it seems that with respect to the user's class accuracy, *sand and gravel (SG)* is mainly confused with *sand and gravel with vegetation*

(SGV) or *bedrock (R)*. Similarly, we also found confusion between *sandy till (sT)* and *bedrock (R).* Confusion between *sand and gravel* and *bedrock* was already observed by Shelat et al. (2012) and by LaRocque et al. (2012). They explained the confusion by the similar multiple scattering characteristics and spectral responses of both classes. Similarly, there is confusion between *sand and gravel with vegetation (SGV)* and *thin till over bedrock* (*T/R).* A similar confusion between sand and gravel and thin till was already observed by LaRocque et al. (2012). All these surficial materials have sparse vegetation cover that is not sufficient to produce strong difference in the volume scattering measured by the HV polarization of RADARSAT-2. It is also not sufficient to produce different Landsat signals, particularly in the blue, green, and red bands that are sensitive to chlorophyll content. Finally, there is confusion between gT and bT. Both are tills and their roughness difference maybe not enough to be detectable with RADARSAT-2 C-HH and C-HV images.

With respect to the producer's accuracy, there is confusion between both *sand and gravel* classes, indicating that the vegetation signal is not enough to make a difference between both classes. The *sand and gravel with vegetation* (*SGV)* class has also confusion with *gravelly till (gT)*. Grunsky et al. (2009) already observed confusion between *sand and gravel* and *thick till* materials. There is some confusion between *bedrock (R)* and *thin till over bedrock (T/R).* Grunsky et al. (2009), LaRocque et al (2012) and Shelat et al. (2012) already documented the difficulty in detecting *thin till* material, mainly because of confusion with the *thick till* class, while in our case, the confusion occurs with the *bedrock* class.

2.6.3 Ground truth accuracies

While being quite high, the accuracies presented in Table 2.8 result from the comparison between the classified image and the training areas. However, such a method only gives an assessment of the classified image accuracy that is different than the true mapping accuracy. A more robust and independent accuracy assessment is to compare the resulting classified image with an independent set of GPS field observation data acquired over the validation sites. For this comparison, we used a total of 1000 GPS sites that were either collected in the field or extracted from air photo-interpretation of helicopter-based pictures and Google Earth images. The GPS sites were selected in order to represent each surficial material class (Table 2.5). If the image returns the same class as the one observed at the validation site, then the pixel related to this validation site is assigned a value of 1. If it is not the case, then the value is zero. Similarly as for the classification accuracies, user's and producer's class accuracies and average and overall accuracies were computed between the ground-truth and the classified image (Table 2.11).

Hereafter, they are referred to as mapping accuracies, as they represent the correspondence between the map resulting from the classified image and the GPS validation sites. A detailed confusion matrix was also produced with the sub-polygon classified image (Table 2.12) and the all-polygon classified image (Table 2.13).

Table 2.11. Ground truth identification accuracies (in %) obtained by comparing the GPS ground observations to the classified image produced by applying the Random Forests Sub-Polygon classifier script to Landsat-8, DEM and slope data, alone or with RADARSAT-2 dual-polarized intensity images (HH and HV).

Class	Sub-Polygon				All-Polygon			
	User's accuracy		Producer's accuracy		User's accuracy		Producer's accuracy	
	Landsat-8	Landsat-8 & Radarsat-2	Landsat-8	Landsat-8 & Radarsat-2	Landsat-8	Landsat-8 & Radarsat-2	Landsat-8	Landsat-8 & Radarsat-2
Ap	78.6	100	84.6	100	89.3	100	89.3	100
Af	60.0	100	100	100	80.0	100	100	100
At	51.9	96.3	82.4	100	37.0	100	71.4	100
O	85.1	87.2	80.0	95.3	89.4	97.9	73.7	95.8
Mc	84.6	100	56.4	100	80.8	100	52.5	100
McV	93.0	100	90.9	97.7	95.3	100	89.1	95.6
Ms	95.7	95.7	74.6	88.0	87.0	93.5	78.4	89.6
MsV	82.4	88.2	77.8	88.2	82.4	94.1	100	100
Ms/R	75.9	85.5	94.0	95.9	77.1	98.8	90.1	97.6
SG	51.6	93.5	64.0	82.9	45.2	93.5	63.6	87.9
SGV	40.6	83.9	36.1	53.1	31.3	90.3	31.3	70.0
T	87.8	92.9	78.2	85.8	86.7	95.9	77.3	89.5
bT	67.5	78.6	81.0	94.3	71.4	86.5	81.1	98.2
cT	50.0	91.7	66.7	88.0	45.8	95.8	68.8	88.5
gT	16.7	70.0	71.4	84.0	16.7	76.7	100	100
gsT	60.0	85.0	80.0	94.4	60.0	85.0	92.3	100
sT	69.6	91.3	76.2	91.3	78.3	87.0	66.7	95.2
TV	61.5	92.3	88.9	100	61.5	100	80.0	100
T/R	90.1	91.2	69.7	86.7	92.4	94.7	72.1	90.5
B	85.1	93.6	97.6	100	87.2	97.9	95.3	100
R	85.1	83.6	78.1	82.4	80.6	86.6	76.1	93.5
Average	**70.1**	**90.5**	**77.5**	**90.9**	**70.3**	**94.0**	**78.5**	**94.9**
Overall	**76.3**	**88.9**	**76.3**	**88.9**	**76.4**	**93.3**	**76.4**	**93.3**

Table 2.12. Confusion matrix (in number of pixels) when comparing GPS ground observations to the classified image produced by applying the Random Forests Sub-Polygon classifier script to Landsat-8, DEM and slope data, alone or with RADARSAT-2 dual-polarized intensity images (HH and HV).

Class	Ap	Af	At	O	Mc	McV	Ms	MsV	Ms/R	SG	SGV	T	bT	cT	gT	gsT	sT	TV	T/R	B	R	User's Accuracy	Error of Omission
Ap	**28**	0	0	0	0	0	0	0	0	0	0	0	0	0	0	0	0	0	0	0	0	100	0.0
Af	0	**5**	0	0	0	0	0	0	0	0	0	0	0	0	0	0	0	0	0	0	0	100	0.0
At	0	0	**26**	0	0	0	0	0	0	1	0	0	0	0	0	0	0	0	0	0	0	96.3	3.7
O	0	0	0	**41**	0	0	0	1	0	0	1	4	0	0	0	0	0	0	0	0	0	87.2	12.8
Mc	0	0	0	0	**26**	0	0	0	0	0	0	0	0	0	0	0	0	0	0	0	0	100	0.0
McV	0	0	0	0	0	**43**	0	0	0	0	0	0	0	0	0	0	0	0	0	0	0	100	0.0
Ms	0	0	0	0	0	0	**44**	0	0	1	1	0	0	0	0	0	0	0	0	0	0	95.7	4.3
MsV	0	0	0	0	0	1	0	**15**	0	0	0	1	0	0	0	0	0	0	0	0	0	88.2	11.8
Ms/R	0	0	0	0	0	0	0	0	**71**	0	3	0	1	0	0	0	0	0	2	0	6	85.5	14.5
SG	0	0	0	0	0	0	0	0	0	**29**	0	0	0	0	0	0	0	0	0	0	2	93.5	6.5
SGV	0	0	0	0	0	0	0	1	0	0	**26**	0	0	0	0	0	0	0	2	0	2	83.9	16.1
T	0	0	0	0	0	0	0	0	1	0	1	**91**	2	0	0	0	0	0	3	0	0	92.9	7.1
bT	0	0	0	1	0	0	0	0	1	3	2	5	**99**	1	4	0	0	0	10	0	0	78.6	21.4
cT	0	0	0	0	0	0	0	0	0	0	0	1	1	**22**	0	0	0	0	0	0	0	91.7	8.3
gT	0	0	0	0	0	0	0	0	0	0	2	2	0	0	**21**	0	0	0	5	0	0	70.0	30.0
gsT	0	0	0	1	0	0	0	0	0	0	0	0	0	1	0	**17**	0	0	1	0	0	85.0	15.0
sT	0	0	0	0	0	0	1	0	0	0	0	0	0	0	0	0	**21**	0	0	0	1	91.3	8.7
TV	0	0	0	0	0	0	0	0	0	0	0	1	0	0	0	0	0	**12**	0	0	0	92.3	7.7
T/R	0	0	0	0	0	0	0	0	1	0	9	0	2	1	0	1	0	0	**156**	0	1	91.2	8.8
B	0	0	0	0	0	0	0	0	0	0	0	1	0	0	0	0	1	0	1	**44**	0	93.6	6.4
R	0	0	0	0	0	0	5	0	0	1	4	0	0	0	0	0	1	0	0	0	**56**	83.6	16.4
Producer's Accuracy	100	100	100	95.3	100	97.7	88.0	88.2	95.9	82.9	53.1	85.8	94.3	88.0	84.0	94.4	91.3	100	86.7	100	82.4		
Error of Commission	0.0	0.0	0.0	4.7	0.0	2.3	12.0	11.8	4.1	17.1	47.9	14.2	5.7	12.0	16.0	5.6	8.7	0.0	13.3	0.0	17.6		

Table 2.13. Confusion matrix (in number of pixels) when comparing GPS ground observations to the classified image produced by applying the Random Forests All-Polygon classifier script to Landsat-8, DEM and slope data, alone or with RADARSAT-2 dual-polarized intensity images (HH and HV).

Class	Ap	Af	At	O	Mc	McV	Ms	MsV	Ms/R	SG	SGV	T	bT	cT	gT	gsT	sT	TV	T/R	B	R	User's Accuracy	Error of Omission
Ap	**27**	0	0	0	0	0	0	0	0	0	0	0	0	0	0	0	0	0	0	0	0	100	0.0
Af	0	**5**	0	0	0	0	0	0	0	0	0	0	0	0	0	0	0	0	0	0	0	100	0.0
At	0	0	**27**	0	0	0	0	0	0	0	0	0	0	0	0	0	0	0	0	0	0	100	0.0
O	0	0	0	**46**	0	0	0	0	0	0	0	1	0	0	0	0	0	0	0	0	0	97.9	2.1
Mc	0	0	0	0	**26**	0	0	0	0	0	0	0	0	0	0	0	0	0	0	0	0	100	0.0
McV	0	0	0	0	0	**43**	0	0	0	0	0	0	0	0	0	0	0	0	0	0	0	100	0.0
Ms	0	0	0	0	0	0	**43**	0	0	1	1	0	0	0	0	0	0	0	0	0	1	93.5	6.5
MsV	0	0	0	0	0	0	0	**16**	0	0	0	1	0	0	0	0	0	0	0	0	0	94.1	5.9
Ms/R	0	0	0	0	0	0	0	0	**82**	0	0	0	0	0	0	0	0	0	1	0	0	98.8	1.2
SG	0	0	0	0	0	0	0	0	0	**29**	0	0	0	0	0	0	0	0	0	0	2	93.5	6.5
SGV	0	0	0	1	0	0	0	0	0	0	**28**	0	0	0	0	0	0	0	2	0	0	90.3	9.7
T	0	0	0	1	0	0	0	0	0	0	0	**94**	1	0	0	0	0	0	2	0	0	95.9	4.1
bT	0	0	0	0	0	0	0	0	2	2	2	6	**109**	0	0	0	0	0	4	0	1	86.5	13.5
cT	0	0	0	0	0	0	0	0	0	0	0	1	0	**23**	0	0	0	0	0	0	0	95.8	4.2
gT	0	0	0	0	0	0	0	0	0	0	1	0	0	0	**23**	0	1	0	5	0	0	76.7	23.3
gsT	0	0	0	0	0	1	0	0	0	0	0	0	0	2	0	**17**	0	0	0	0	0	85.0	15.0
sT	0	0	0	0	0	0	0	0	0	0	0	0	0	0	0	0	**20**	0	3	0	0	87.0	13.0
TV	0	0	0	0	0	0	0	0	0	0	0	0	0	0	0	0	0	**13**	0	0	0	100	0.0
T/R	0	0	0	0	0	0	0	0	0	0	7	0	1	1	0	0	0	0	**162**	0	0	94.7	5.3
B	0	0	0	0	0	0	0	0	0	0	0	1	0	0	0	0	0	0	0	**46**	0	97.9	2.1
R	0	0	0	0	0	1	5	0	0	1	1	1	0	0	0	0	0	0	0	0	**58**	86.6	13.4
Producer's Accuracy	100	100	100	95.8	100	95.6	89.6	100	97.6	87.9	70.0	89.5	98.2	88.5	100	100	95.2	100	90.5	100	93.5		
Error of Commission	0.0	0.0	0.0	4.2	0.0	4.4	10.4	0.0	2.4	12.1	30.0	10.5	2.8	12.5	0.0	0.0	4.8	0.0	9.5	0.0	6.5		

When only Landsat-8 data are used in the RF classification, the mapping overall accuracy is 76.3% for the *Sub-polygon* script and 76.4% with the *All-polygon* script (Table 2.11). As for the J-M distances and the classification accuracies, adding RADARSAT-2 in the classification strongly improves the mapping overall accuracies which increase from 76.3% to 88.9% in the case of the *sub-polygon* script and from 76.4% to 93.3% in the case of the *all-polygon* script. Since the combination of Landsat-8 and RADARSAT-2 gives the best classification accuracies, we will only present and discuss this case for the remaining of the section.

The related confusion matrices are shown in Table 2.12 for the *sub-polygon* script and in Table 2.13 for the *all-polygon* script. With the *sub-polygon* script, all the classes have a user's and producer's class mapping accuracy above 90%, except eight classes in the case of the user's class mapping accuracy and nine classes in the case of the producer's class mapping accuracy. The highest errors of omission occur with *gravelly till (gT)* (30%) and *bouldery till (bT)* (21.4%), in both cases mainly because of confusion with *thin till over bedrock* (*T/R).* Other classes showing errors of omission higher than 10% are *bedrock (R)* (16.4% or 3 sites) and *sand and gravel with vegetation (SGV)* (16.1% or 3 sites), both classes being confused with each other. High errors of omission also occur with *gravelly sandy till (gsT)* (15.0% or 17 sites), *thin marine sand (Ms/R)* (14.5% or 71 sites), *organic (O)* (12.8% or 41 sites), and *marine sand with vegetation (MsV)* (11.8% or 15 sites). For *gsT*, a small confusion occurs with *organic (O)* at one site, with *carbonate till (cT)* at one site, and with *thin till over bedrock* (*T/R)* at one site. For *Ms/R*, the confusion occurs with *bedrock (R)* (6 sites). Both the *organic (O)* (12.8% or 4 sites), and *marine sand with vegetation (MsV)* (11.8% or one site) classes are confused with the

thick till (T) class, *MsV* being also confused with *McV* at one 1 site. *Sand and gravel with vegetation (SGV)* has the highest error of commission (47.9% or 26 sites), mainly because of confusion with *bedrock (R)* and *sand and gravel (SG).* The second error of commission occurs for *bedrock (R)* (17.6% or 56 sites) that is confused with *thin marine sand (Ms/R).* Five classes have confusion with *bouldery till (bT)* that leads to high error of commission: *sand and gravel (SG)* (17.1% or 29 sites), *gravelly till (gT)* (16.0% or 21 sites), *thick till (T) (*14.2% or 91 sites), *thin till over bedrock* (*T/R)* (13.3% or 156 sites), and *carbonate till (cT)* (12.0% or 22 sites). Both the marine sand classes (*Ms* and *MsV*) have also a high error of commission (12.0% and 11.8%, respectively). For *Ms*, the confusion occurs with *bedrock (R).* For *MsV,* the confusion occurs with *organic (O)* at 1 site and *sand and gravel with vegetation (SGV)* at 1 site.

With the *all-polygon* script, all the classes have a mapping user's and producer's class accuracy higher than with the *sub-polygon* script, except for the user's class accuracy in the case of *marine sand (Ms)* and of *sandy till (sT)* and for the producer's class accuracy, in the case of *offshore silt and clay with vegetation (McV).* All the user's and producer's class accuracies are above 90%, except for five classes in the case of both the user's class accuracy and the producer's class accuracy. The highest error of omission occurs for *gravelly till (gT)* (23.3% or 23 sites), followed by *gravelly sandy till (gsT)* (15.0% or 17 sites), *bouldery till (bT)* (13.5% or 109 sites), *bedrock (R)* (13.4% or 58 sites), and *sandy till (sT)* (13.0% or 20 sites). *sT, bT,* and *gT* are confused with *thin till over bedrock* (*T/R),* bT being also confused with *thick till (T). gsT* is confused with *carbonate till (cT)* and *bedrock (R)* with *marine sand (Ms).* The highest error of commission occurs with *sand and gravel with vegetation (SGV)* (30%) because of confusion with *thin till*

over bedrock (*T/R)* at 7 sites. The other high errors of commission are for *sand and gravel (SG)* (12.1%) because of a confusion with *bouldery till (bT)* (2 sites), for *carbonate till (cT)* (11.5%) because of confusion with *gravelly sandy till (gsT)* (2 sites), for *thick till (T)* (10.5%) because of confusion with *bouldery till (bT)* (6 sites), and for *marine sand (Ms)* (10.4%) because of confusion with *bedrock (R)* (5 sites).

Regardless of the script used, the user's class and producer's class accuracies are higher than 90%. Despite these high-class mapping accuracies, it seems that with respect to the user's class accuracy, *gravelly till (gT), gravelly sandy till (gsT), bouldery till (bT),* and *bedrock (R)* have high errors of omission. *Gravelly till (gT)* and *bouldery till (bT)* are mainly confused with *thin till over bedrock* (*T/R).* Probably all these till materials have multiple scattering characteristics and spectral responses that are too similar to be detected on the Landsat-8 and RADARSAT-2 C-HH and C-HV images. *Gravelly sandy till (gsT)* is mainly confused with *carbonate till (cT),* but confusion also occurs with *organic (O)* and *thin till over bedrock* (*T/R)* in the case of the sub-polygon script. *Bedrock (R)* is mainly confused with *sand and gravel with vegetation (SGV)* in the case of the *sub-polygon* script and with the *marine sand (Ms)* in the case of the *all-polygon* script.

With respect to the producer's accuracy, there is confusion between *sand and gravel with vegetation (SGV)* and either *sand and gravel (SG)* or bedrock-related classes (*R* or *T/R*), indicating that the vegetation signal is not important enough to make a difference between these classes. The *sand and gravel* (*SG)* class is also confused with *bouldery till (bT)* which is also confused with *thick till (T), thin till over bedrock (T/R),* and *gravelly till (gT). Sand and gravel* has already shown to be confused with *thick till* (Grunsky et

al. 2009), *thin till* (LaRocque et al. 2012) and with *bedrock* (Shelat et al. 2012). There is some confusion between *bedrock (R)* and *marine sand (Ms)* or *thin marine sand (Ms/R). Carbonate till (cT)* is confused with several other till classes, mainly with *gravelly sandy till (gsT)* but also with *bouldery till* (*bT*) and *thin till over bedrock (T/R)*.

2.7 CONCLUSIONS

A surficial material map with 21 classes was produced for an area north of Wager Bay in Nunavut using a non-parametric classifier, *Random Forests* (RF), which was applied to a combination of RADARSAT-2 C-band dual- polarized (HH and HV) and Landsat-8 OLI images with a digital elevation model and slope data. Two versions of Random Forests were tested: the *all-polygon* and *sub-polygon* versions. The resulting map was compared to about 1000 GPS sites with field observations or interpreted from air photo interpretation/Google Earth to determine its mapping accuracy. We showed that adding RADARSAT-2 C-HH and C-HV images to the classifier significantly improves both the classification and mapping accuracies. The overall accuracy increases from 90.6% to 96.4% with the *sub-polygon* script and from 92.8% to 98.1% with the *all-polygon* script. Similarly, the mapping accuracy increases from 76.3% to 88.9% with the sub-polygon script and from 76.4% to 93.3% with the all-polygon script. Besides the overall accuracies, the *all-polygon* script also resulted in higher user's and producer's classification and mapping accuracies for the majority of l classes. With the *all-polygon* script, all the classification accuracies were higher than 95% in the case of both the user's and producer's accuracies for each individual class However six classes have user's accuracies higher than 89% (*sandy till (sT), gravelly till (gT),* and both *sand and gravel* classes *(SG and SGV)).* Similarly, the mapping user's and producer's accuracies

are above 85% for all individual classes, except the user's accuracy of the *gravelly till (gT) class* (76.7%) and the producer's accuracy of the *sand and gravel with vegetation (SGV)* class (70%). In both cases, the confusion mainly occurred with *thin till over bedrock* (*T/R).*

The RADARSAT-2 were acquired in two orbits (ascending and descending) giving an east and west-looking direction and under two different environmental conditions (wet and dry), but all the images have the same incidence angles (between 20 and 49.3°) because of the limited availability of RADARSAT-2 images. Further work is needed to include in the classification RADARSAT-2 images acquired under different incidence angles, as Shelat et al, (2012) already showed that the combination of steep, medium and shallow incidence angles increases class separability and classification accuracies in the case of surficial materials mapping. Our study also uses only HH and HV images and the addition of VV images may improve the accuracies, as shown by Shelat et al. (2012) to facilitate the differentiation between surficial materials, for example between *thick till with vegetation* and *sand and gravel*. RADARSAT-2 can also provide polarimetric images, which also have the phase information providing an additional opportunity to develop improved tools for mapping surficial materials, such as polarization synthesis, polarimetric variables, polarimetric decomposition parameters, polarimetric signatures of target materials. The use of RADARSAT-2 polarimetric images for mapping surficial materials needs to be further examined. Finally, our study only uses C-band SAR images and the use of SAR images acquired in longer wavelengths such as Alos-PalSAR L-band SAR images could represent a valuable research avenue.

2.8 REFERENCES

Breiman, L. 2001: Random forests; Machine Learning, 45(1), 5–32.

Breiman, L. 2003: Manual of setting up, using and understanding random forests, V4.0; University of California Berkeley, Berkeley, California, 33 p., URL <http://www.stat.berkeley.edu/~breiman/Using_random_forests_v4.0.pdf> [November 2015].

Brown, O., Harris, J.R. and Utting, D. 2008: Case study 6: surficial mapping of northern Baffin Island using Landsat and topographic data; *in* Remote Predictive Mapping: An Aid for Northern Mapping, J.R. Harris (ed.), Geological Survey of Canada, Open File 5643, p. 225–232.

Byatt, J. 2014: Influence of environmental conditions on surficial deposit mapping using Landsat-5 TM and RADARSAT-2 polarimetric SAR images; B.Sc. (honour) thesis, University of New Brunswick, Fredericton, New Brunswick, 24 p.

Byatt, J. La Rocque, A., Leblon, B.,Harris, J., and McMartin, I. 2017. Mapping surficial materials in Nunavut using RADARSAT-2 C-HH and C-HV, Landsat-8 OLI, DEM, and slope data. Part 2 - South of Wager Bay area, International Journal of Remote Sensing (submitted)

Campbell, J.E., Harris, J.R., Huntley, D.H., McMartin, I., Wityk, U., Dredge, L.A. and Eagles, S. 2013: Remote predictive mapping of surficial earth materials: Wager Bay north area, Nunavut - NTS 46-E (N), 46-K (SW), 46-L, 46-M (SW), 56-H (N), 56-I and 56-J (S); Geological Survey of Canada, Open File 7118, 42 p.

Gislason, P., Benediktsson, J. and Sveinsson, J. 2006: Random forest for land cover classification; Pattern Recognition Letters, v. 27, p. 294–300.

Goodman J.W. 1976: Some fundamental properties of speckles; Journal of Optical Society of America, 66(11), 1145–1150.

Google 2015: Google Maps™ satellite image of Wager Bay, Nunavut; Google, image, URL <http://maps.google.ca/maps> [©2015 Google - Imagery, ©2015 Data SIO, NOAA, US Navy, NGA, GEBCO, Landsat, IBCAO Map data, November 2015].

Grunsky, E., Harris, J.R. and McMartin, I. 2009: Predictive mapping of surficial materials, Schultz Lake area (NTS 66 A), Nunavut, Canada; Reviews in Economic Geology, 16, 177–198.

Harris, J.R. 2008: What is RPM: chapter 1; *in* Remote Predictive Mapping: An Aid for Northern Mapping, J.R. Harris (ed.), Geological Survey of Canada, Open File 5643, p. 1–4.

Harris, J.R., Grunsky, E. and Singhroy, V. 2008a: Radar remote sensing; *in* Remote Predictive Mapping: An Aid for Northern Mapping, J.R. Harris (ed.), Geological Survey of Canada, Open File 5643, p. 135–160.

Harris, J.R., Grunsky, E. and McMartin, I. 2008b: Classification of remotely sensed imagery for surficial geological mapping in Canada's north, Case 7; in Remote Predictive Mapping: An Aid for Northern Mapping, J.R. Harris (ed.), Geological Survey of Canada, Open File 5643, p. 233–244.

Harris, J.R., Wickert, L., Lynds, T., Behnia, P., Rainbird, R., Grunsky, E., McGregor, R. and Schetselaar, E. 2011: Remote predictive mapping 3. Optical remote sensing – a

review for remote predictive mapping in northern Canada, Geoscience Canada, v. 38, p. 49–83.

LaRocque, A., Leblon, B., Harris, J.R., Jefferson, C.W., Tschirhart, V. and Shelat, Y. 2012: Surficial materials mapping in Nunavut, Canada, with multi-beam RADARSAT-2 dual-polarization C-HH and C-HV, Landsat-7 ETM+, and DEM data; Canadian Journal of Remote Sensing, 38, 281–305.

LaRocque, A., Yue, B., Leblon, B., Haddadi, A., Harris, J., Jefferson, C. and Shelat, Y. 2013: A comparison of supervised classifiers applied to RADARSAT-2 polarimetric SAR and Landsat-7 ETM+ images for mapping surficial materials in Nunavut; 34th Canadian Remote Sensing Symposium, August 27–29, 2013, Victoria, British Columbia, Program with Abstracts.

Louppe, G., Wehenkel, L., Sutera, A. and Geurts, P. 2013: Understanding variable importances in forests of randomized trees; Advances in Neural Information Processing Systems, 26, 431–439.

McMartin, I. and Dredge, L.A. 2005: History of ice flow in the Shultz Lake and Wager Bay areas, Kivalliq Region, Nunavut; Geological Survey of Canada, Current Research 2005-B2, 10 p.

McMartin, I., Campbell, J.E., Dredge, L.A., LeCheminant, A.N., McCurdy, M.W., and Scromeda, N., 2015a. Quaternary geology and till composition north of Wager Bay, Nunavut: results from the GEM Wager Bay Surficial Geology Project; Geological Survey of Canada, Open File 7748, 58 p.

McMartin, I., Byatt, J., Randour, I., and Day, S.J.A., 2015b. Report of 2015 activities for regional surficial mapping, till and stream sediment sampling in the Tehery-Wager GEM 2 Rae Project area; Geological Survey of Canada, Open File 7966, 14 p.

McMartin, I., Day, S.J.A., Randour, I., Roy, M., Byatt, J., LaRocque, A. and Leblon, B., 2016. Report of 2016 activities for the surficial mapping and sampling surveys in the Tehery-Wager GEM-2 Rae Project area; Geological Survey of Canada, Open File 8134, 16p.

Mei, S. and Paulen, R.C. 2009: Using multi-beam RADARSAT-1 imagery to augment mapping surficial geology in northwest Alberta, Canada; Canadian Journal of Remote Sensing, 35, 1–22.

Natural Resources Canada 2015: Canadian digital elevation data, Level 1, Natural Resources Canada, URL <http://geogratis.gc.ca/api/en/nrcan-rncan/ess-sst/C40ACFBA-C722-4BE1-862E-146B80BE738E.html> [April 2015].

Ou, C., LaRocque, A., Leblon, B. Yu, Z., Webster, K., McLaughlin, J. 2016: Mapping permafrost using RADARSAT-2 and Landsat images, 2 – Regional mapping, International Journal of Remote Sensing, 37(12): 2751-2779

Ozdarici-Ok, A., Akar, O. and Gungor, O. 2012: Evaluation of random forest method for agricultural crop classification; European Journal of Remote Sensing, 45, 421–432.

R Development Core Team 2012: R: a language and environment for statistical computing; software development tools, R Foundation for Statistical Computing, Vienna, Austria, URL <http://www.R-project.org/> [November 2015].

Schetselaar, E.M., Harris, J.R., Lynds, T. and de Kemp, E.A. 2007: Remote predictive mapping 1. Remote predictive mapping (RPM): a strategy for geological mapping of Canada's north; Geoscience Canada, 34, p. 93–111.

Shelat, Y., Leblon, B., LaRocque, A., Harris J., Jefferson, C. W., Lentz, D., and Tschirhart, V. 2012b. Effects of incidence angles and image combinations on mapping accuracy of surficial materials in the Umiujalik Lake area, Nunavut using RADARSAT-2, polarimetric and Landsat 7 images, and DEM data. Part 1. Non-Polarimetric Analysis. Canadian Journal of Remote Sensing, 38(3): 383-403

Smith, C.A.S., Meikle, J.C., and Roots, C.F. (editors), 2004. Southern arctic ecozone. In *Ecoregions of the Yukon Territory - Biophysical Properties of Yukon Landscapes.* Agriculture and Agri-Food Canada, PARC Technical Bulletin 04-01, Summerland, British Columbia, pp. 61 - 72.

Strobl, C., Boulesteix, A.L., Kneib, T., Augustin, T. and Zeileis, A. 2008: Conditional variable importance for random forests; BMC Bioinformatics, 9:307, 11 p.

United States Geological Survey 2015: Landsat 8 (L8) data users handbook; Sioux Falls, South Dakota, EROS, June 2015, 9 p., URL <https://landsat.usgs.gov/documents/Landsat-8DataUsersHandbook.pdf> [November 2015].

Waske, B. and Braun, B. 2009: Classifier ensembles for land cover mapping using multi-temporal SAR imagery; ISPRS Journal of Photogrammetry and Remote Sensing, 64, 450–457.

Wityk, U., Harris, J.R., McMartin, I., Campbell, J.E., Ross, M., and Grunsky, E., 2013. Remote predictive mapping of surficial materials, West of Repulse Bay, Nunavut (NTS 46M-SW, 46L-W and -S, 46K-SW), GSC Open File 7357, 20 pages and appendices

CHAPTER 3[2]

MAPPING SURFICIAL MATERIALS IN NUNAVUT USING RADARSAT-2 C-HH AND C-HV, Landsat-8 OLI, DEM AND SLOPE DATA. PART 2 - SOUTH OF WAGER BAY AREA

3.1 ABSTRACT

Responsible resource management requires accurate and detailed geological maps. This is the goal behind current efforts to map surficial materials in the Canadian Arctic, which is important for planning and managing natural resources, including minerals and energy. The area south of Wager Bay, Nunavut (NTS map sheets 046D, E, 055P, 056A, H) is the subject of an intensive surficial geology mapping project. For this study area, a map detailing 22 surface materials classes was produced using a non-parametric classifier, Random Forests (RF), applied to a combination of RADARSAT-2 C-band dual- polarized (HH and HV) and Landsat-8 OLI images with a digital elevation model and slope data. We show that the addition of RADARSAT-2 C-HH and C-HV images in the classification process increases the overall classification accuracy from 96.7% to 99.3%. Similarly, the accuracy determined by comparing the resulting maps with georeferenced field data (called hereafter mapping accuracy) increases from 72.1% to

2. [2] Byatt, J., LaRocque, A., Leblon, B., Harris, J., and McMartin, I. 2017. Mapping surficial materials in Nunavut using RADARSAT-2 C-HH and C-HV, Landsat-8 OLI, DEM, and slope data. Part 2 - South of Wager Bay area, International Journal of Remote Sensing (submitted)

78.0% when RADARSAT-2 C-HH and C-HV images are added to the classification. The classes with the highest mapping accuracies were *flooded alluvium* and *boulders*, both with 100%. The class with the lowest mapping accuracy was *thin sand and gravel over bedrock* (11.1%), commonly confused with *sand and gravel with vegetation* and *bedrock.*

3.2 INTRODUCTION

Surficial geological mapping is traditionally based on the interpretation of aerial photographs using a stereoscope, ground-truthed by field work. However in Arctic regions, field surveys are time-consuming and costly because of the remote access and the lack of infrastructure for logistical support. To address these limitations and assist in the interpretation of the surficial geology, an innovative method for mapping surficial materials is the use of satellite imagery in concert with digital image processing techniques. This approach offers the advantages of extensive regional coverage, no disturbance of the areas to be mapped, as well as complete and cost effective data coverage. Optical images such as Landsat or SPOT can be used (i.e. Harris et al., 2011), but optical images cannot be acquired at night or during cloudy conditions. These limitations do not exist with synthetic aperture radar (SAR) images, such as those acquired by RADARSAT-2 (e.g., Schetselaar et al., 2007; LaRocque et al., 2012), because SAR is an active sensor that generates its own microwave energy and therefore image acquisition is independent of atmospheric conditions, although image quality can be affected by ground moisture related to weather and climate.

Previous research using SAR images for mapping surficial materials of the Canadian North was limited largely to single frequency and single polarization sensors on board of RADARSAT-1 (Harris et al., 2008a; Grunsky et al., 2009; Mei and Paulen, 2009). More recent studies have employed the advantages of multipolarized SAR images, particularly the dual combination of like- and cross- polarized data (LaRocque et al., 2012; Shelat et al., 2012; Byatt et al. 2017). Cross-polarized images can measure depolarization over areas of vegetation (Evans et al., 1986) and extreme surface roughness (Schaber et al., 1997). Combining SAR and optical imagery offers several advantages because both image types are complementary (Grunsky et al. 2009; Mei and Paulen, 2009; Shelat et al. 2012; LaRocque et al., 2012; Byatt et al. 2017). SAR images are sensitive to surface texture by providing information on scattering mechanisms that are related to surface roughness and moisture content (Harris et al., 2008b; LaRocque et al., 2012). Optical images are sensitive to surficial reflective properties that are generally governed by surface chemistry, vegetation, and surface moisture content (Brown et al., 2008).

The study is part of a surficial geology mapping effort under Natural Resources Canada's Geo-mapping for Energy and Minerals (GEM1 and 2) program to provide new geological knowledge on the nature and composition of surficial materials for sustainable resource development and land-use management in central mainland Nunavut (McMartin et al., 2013, 2015a, b, 2016). The study is subdivided into two parts. Part 1 (Byatt et al., 2017) produced a surficial materials map with 21 classes for an area located north of Wager Bay by applying a non-parametric supervised classifier (*Random Forests*) to a combination of Landsat 8 optical images and RADARSAT-2 SAR C-HH and C-HV images as well as a digital elevation model (DEM) and derived slope data.

This paper (Part 2) will apply the same methodology developed and validated in the area north of Wager bay to produce a surficial materials map comprising 22 classes for an area located south of Wager Bay, Nunavut, as part of the GEM-2 Tehery-Wager Activity within the Rae Project area. The resulting map will be validated with an independent set of GPS field data that were acquired in summers of 2012, 2015, and 2016.

3.3 STUDY AREA

The study area is located south of Wager Bay, Nunavut, on the western side of Hudson Bay and includes parts of Ukkusiksalik National Park (Figure 3.1). It covers the NTS map sheets 046D, E, 055P, 056A, H. The digital elevation model of Figure 3.1 shows that elevations range from sea level along Wager Bay and Hudson Bay to 550 m amsl in the northwestern part of the study area. The drainage network links numerous intermediate to large lakes and ponds (Figure 3.1). The overall discharge direction of drainage systems is from west to east through Roes Welcome Sound and Daly Bay into Hudson Bay, or south to north for the uplands that slope abruptly into Wager Bay (Figure 3.1). As reported in Byatt et al. (2017), the climatic conditions in the study area are related to an arctic climate. The related vegetation is typical of the Arctic tundra and is mainly composed of dwarf shrubs, birch, willow mixed with herbs, lichens, and mosses (Smith et al., 2004). Soils in the lowland areas are organic soils (peat), whereas other soils are cryosols associated with deep permafrost (frozen soil) and related periglacial landforms (Smith et al., 2004). However, the top layer of frost soil thaws during the summer, can create standing water and/or saturated soils, which may interfere with radar backscatter (Byatt et al. 2017)

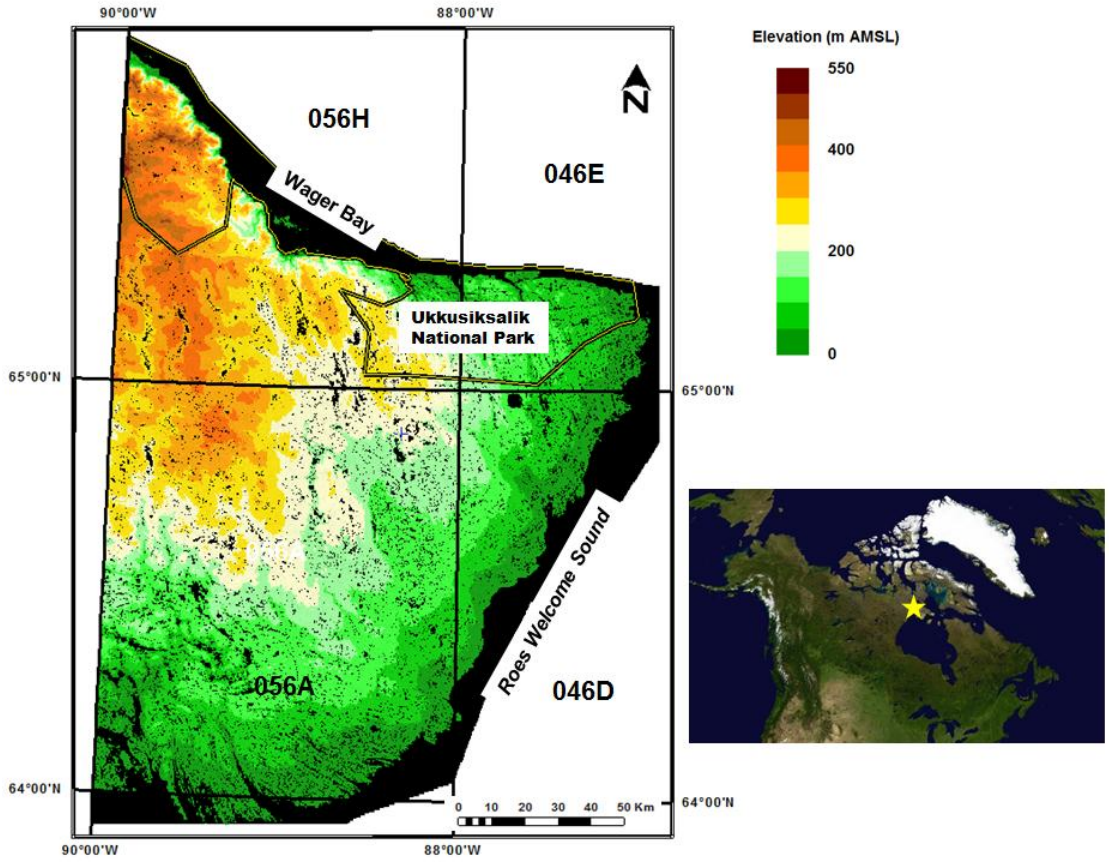

Figure 3.1. Location and digital elevation model for the study area located south of Wager Bay, Nunavut. Abbreviations: amsl, above mean sea level.

From a surficial geology point of view, the area is characterized by streamlined, thin and thick till extending southeast from a major ice divide zone (Keewatin Ice Divide), from which ice flowed radially during the last glaciation (McMartin and Dredge, 2005). The former Keewatin Ice Divide zone, centred in the uplands southwest of Wager Bay, is now dominated by a mixture of till blankets and veneers, felsenmeer, and weathered bedrock (McMartin et al., 2013, 2015b, 2016). This glacial landscape is interspersed by a complex system of subglacial meltwater corridors and proglacial channels. The subglacial corridors comprise large eskers, outwash plains, small irregular hummocks and ridges of sandy diamicton, short streamlined landforms of till, boulder lags, and

washed bedrock surfaces. Where proglacial meltwater systems abound, till surfaces show extensive erosion and/or reworking. Between the corridors and away from proglacial channels, till surfaces show no sign of glaciofluvial erosion or reworking. The limit of postglacial marine submergence increases from 119 m amsl south of Wager Bay to about 145–160 m amsl west of Roes Welcome Sound. Lowlands that skirt the coasts of Roes Welcome Sound and Daly Bay, to the south, show evidence of postglacial marine erosion and reworking of thin glacial and glaciofluvial sediments. Marine veneers are sandy and occur as scattered deposits between rock ridges or glacial landforms. Preliminary surficial geology maps compiled at the 1:100, 000 scale as part of the GEM program in NTS 46D and 56A prior to field work (Dredge et al., 2013a, b, c) are based largely on air-photo interpretation with little ground-truthing. In NTS 56H-south, Randour and McMartin (in press) more recently compiled a surficial geology map based on detailed field observations.

3.4 MATERIALS

We used five Landsat-8 images acquired over two years from 2013 to 2014 by the *Operational Land Imager* (OLI) sensor (Table 3.1). They were mosaicked together to cover the entire study area. They were visually checked to ensure that the ground was free of ice and snow. These images do not include any clouds or shadows. The Landsat 8 images were already georeferenced in a NAD83 format (UTM Zone 16, Row W) and have eight bands: B1 (0.43–0.45 µm), B2 (0.45–0.51 µm), B3 (0.53–0.59 µm), B4 (0.64–0.67 µm), B5 (0.85–0.88 µm), B6 (1.57– 1.65 µm), B7 (2.11–2.29 µm), and B8 (0.50–0.68 µm).

Table 3.1 Characteristics of the Landsat-8 OLI images used for this study on Wager Bay south.

Image ID	Date	Time UTC	Cloud cover (%)	Sun elevation (°)	Sun azimuth (°)	Precipitation (mm)(*)
LC80310142013207LGN00	2013/07/26	17h19	0.71	43.40	167.48	0.42
LC80310142013223LGN00	2013/08/11	17h19	2.35	39.23	168.42	0.20
LC80330132013221LGN00	2013/08/09	17h32	1.28	41.04	166.57	0.62
LC80330142013221LGN00	2013/08/09	17h31	0.01	39.81	166.26	0.62
LC80340132014247LGN00	2014/09/04	17h35	0.04	30.03	172.08	16.42

(*) Total of rain equivalent (in mm) during the three days prior to image acquisition, estimated from the mean precipitation recorded at Baker Lake (*64°19′05″N 096°01′03″W),* Rankin Inlet (62°48′35″N 092°05′58″W), Kugaaruk (68° 32' 0"N, 89° 49' 0"W), Gjoa Haven (68°37′33″N 095°52′30″W), and Hall Beach (68°46′38″N 081°13′27″W)

Eight RADARSAT-2 Scan SAR Wide-A C-band dual-polarized (HH and HV) imags acquired in August of 2014 were used for this study (Table 3.2). They were acquired with an incidence angle that varied between 20 and 49.3°. Four SAR images were acquired with an ascending orbit resulting in an east-looking direction and four with a descending orbit resulting in a west-looking direction (Table 3.2). While the ascending orbit images were acquired during dry conditions, the descending orbit images were acquired during dry and wet conditions, as Byatt (2014) showed that the accuracy of surficial material maps increases when optical and SAR images acquired over dry and wet conditions are combined. Each image file had two images: the HH polarized image and the HV polarized intensity image. All the images were checked visually to ensure the ground was free of snow and ice cover.

Table 3.2. Characteristics of the RADARSAT-2 dual polarized (C-HH and C-HV) images used for this study in Wager Bay south.

Image ID	Orbit	Date	Local time	Precipitation (mm)	Mosaic ID
RS2_20140815_SCWA_A1 **RS2_20140815_SCWA_A2**	Ascending	15/08/2014	18h21	2.04	A2
RS2_20140825_SCWA_A1 **RS2_20140825_SCWA_A2**	Ascending	25/08/2014	18h30	0.22	A4
RS2_20140814_SCWA_D1 **RS2_20140814_SCWA_D2**	Descending	14/08/2014	12h19	6.06	D2
RS2_20140824_SCWA_D1 **RS2_20140824_SCWA_D2**	Descending	24/08/2014	12h27	0.18	D4

(*) Total of rain equivalent (in mm) during the three days prior to image acquisition, estimated from the mean precipitation recorded at Baker Lake (*64°19′05″N 096°01′03″W)*, Rankin Inlet (62°48′35″N 092°05′58″W), Kugaaruk (68° 32' 0"N, 89° 49' 0"W), Gjoa Haven (68°37′33″N 095°52′30″W), and Hall Beach (68°46′38″N 081°13′27″W)

Ancillary data used in this study included several 1:50 000 DEM tiles that were downloaded from GeoGratis (Natural Resources Canada, 2015). They that were used for terrain correction when georeferencing the SAR images and for correcting the topographic effects in the mosaicking process. The DEM has a resolution of 16.1 m in the x direction, 23.3 m in the y direction and 1 m in the z direction. Ground elevations are recorded in meters relative to mean sea level (amsl), based on the NAD83 horizontal reference datum.

Three types of GPS sites were used in the study. The first one consists of field observations collected at 45 sites during the summer of 2015 as part of a GEM-2 funded project (Byatt et al., 2015). These were carefully selected to cover most of the surficial materials classes. The second one comprises field observations collected by surficial geologists over 118 sites during the summers of 2012, 2015, and 2016 as part of a GEM-1 and GEM-2 funded projects (McMartin et al., 2013, 2015b, 2016). They consist of

ground pictures, GPS coordinates and descriptions of the surficial deposits and landforms, reclassified into one of the 22 surface material classes as best as possible by the field geologist. The third type of GPS sites were determined from photo-interpretation of helicopter-based pictures collected in 2015 and Google Earth images. Altogether, the study used 1168 GPS sites. Among them, 514 sites were used to delineate training polygons of at least 10 pixels and about 654 GPS sites were used to validate the produced map. Both the training and validation GPS sites were all well distributed across the study area (Figure 3.2). Details on the distribution of the training and validation GPS sites within the surficial material classes are presented in the *Image classification* section.

3.5 METHODS

3.5.1 Image processing

The flowchart presented in Figure 3.3 provides a summary of the image processing methodology used in the study. The majority of the image processing was performed in *PCI Geomatica* 2015 software. The DEM tiles were first imported and then mosaicked together using the *OrthoEngine* module of *PCI Geomatica*. The digital numbers of the Landsat 8 OLI images were first converted into top of atmosphere (TOA) reflectance values, following the method described in the Landsat 8 users handbook (United States Geological Survey, 2015). This conversion also removes some of the atmospheric interferences.

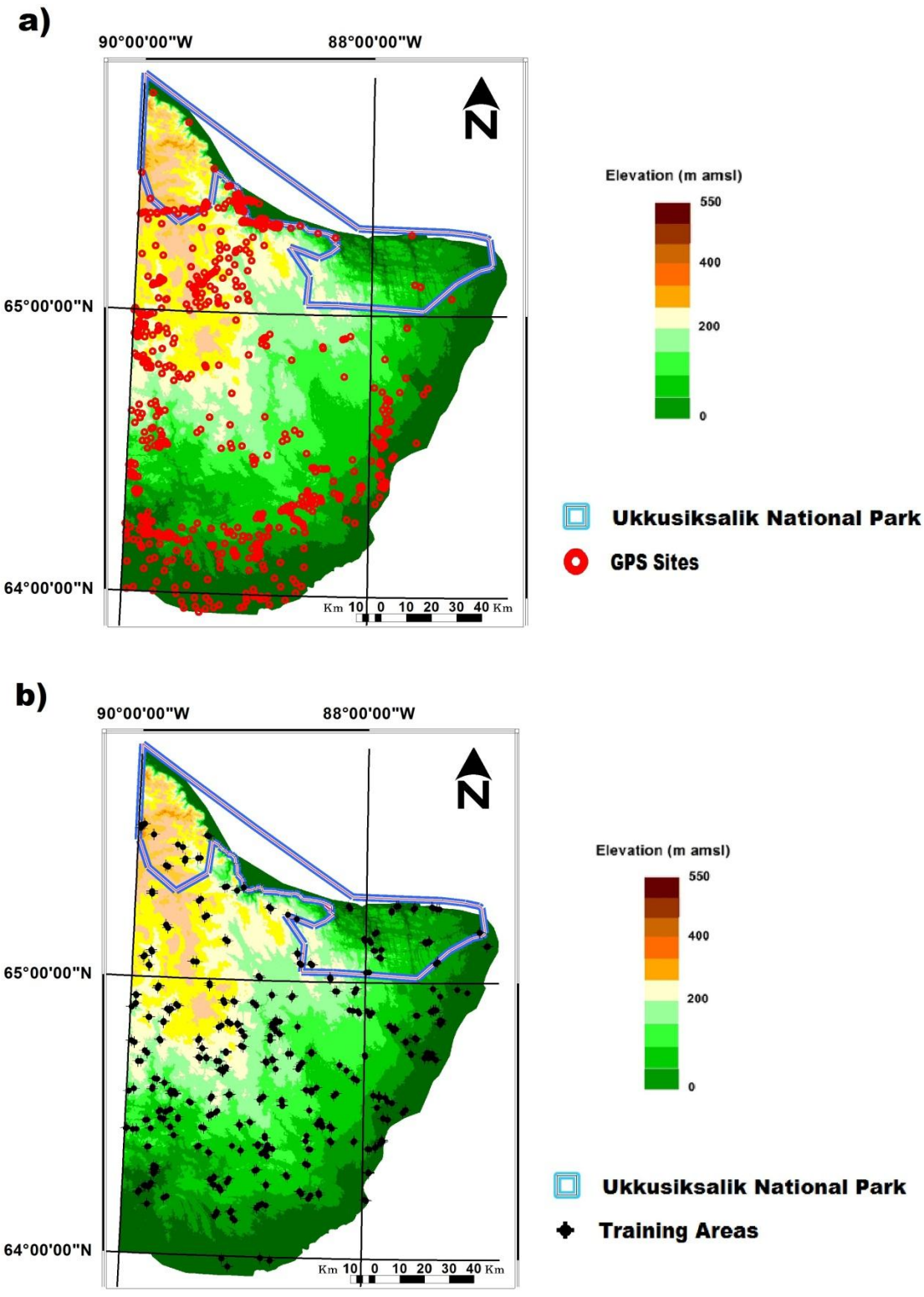

Figure 3.2. Location of a) the GPS validation sites and b) training areas in the Wager Bay south.

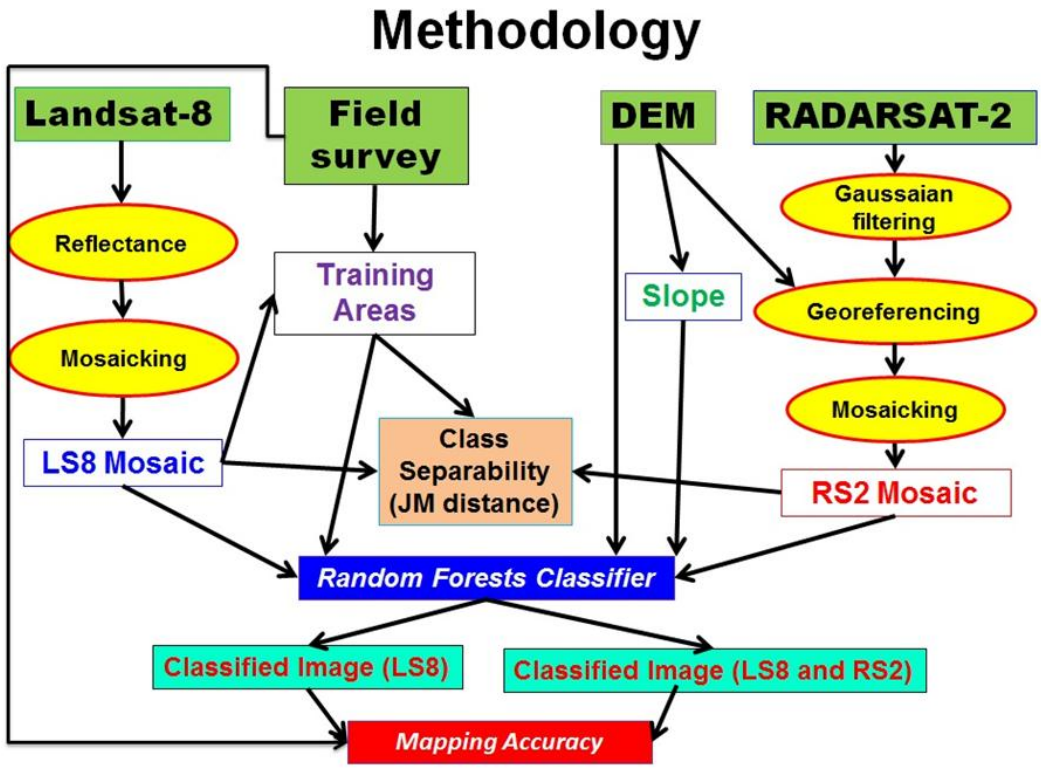

Figure 3.3. Flowchart describing the methodology of the study.

Following LaRocque et al. (2012), the RADARSAT-2 C-HH and C-HV images were filtered to help suppress the effects of speckle using a Gaussian filter (with a standard deviation of 1.6) following the method of Grunsky et al. (2009). Speckle is a multiplicative noise and its intensity must be attenuated in order to enhance fine details on SAR images (Goodman, 1976). Each individual image was then orthorectified with the *"RADARSAT-2 Rational Function Model"* function provided by the *Orthoengine* module of *PCI Geomatica*, using the DEM and ground control points (GCPs). Approximately 20 GCPs were extracted from the orthorectified Landsat 8 data for

georeferencing, achieved with a mean accuracy of less than one pixel in both x and y axes (Table 3.3). The georeferenced images were then mosaicked together to cover the entire study area. This was accomplished using the *OrthoEngine* module of *PCI Geomatica*, using the "*Automatic Mosaicking*" menu that requires the use of the DEM. The parameters used in the mosaicking method were as follows: histogram for the full image, adaptive filter: 20 % of the image, match area: 10 %, cutline: minimum difference, and blend width: 20 pixels.

Table 3.3. Orthorectification accuracy (in pixel) of the RADARSAT-2 images used in this study.

Image ID	Number of ground control points	RMS error		
		X	Y	Mean
RS2_20140815_SCWA_A1	18	0.77	0.54	0.55
RS2_20140815_SCWA_A2	15	0.84	0.6	0.59
RS2_20140825_SCWA_A1	24	1.09	0.76	0.78
RS2_20140825_SCWA_A2	12	0.78	0.59	0.52
RS2_20140814_SCWA_D1	13	0.82	0.58	0.58
RS2_20140814_SCWA_D2	20	0.70	0.49	0.50
RS2_20140824_SCWA_D1	20	0.75	0.44	0.60
RS2_20140824_SCWA_D2	20	0.50	0.58	0.77

3.5.2 Image classification

We used the same surficial material classes as for the Wager Bay North area (Byatt et al. 2017), with some exceptions (Table 3.4). One surface materials class used in the Wager Bay North study, that of *carbonate-rich till* (cT), was not used in the southern region because it was not present south of Wager Bay (McMartin et al., 2015b). Two additional surficial materials classes, *thin sand and gravel over bedrock (S/T)*, and *wave-washed till* (wT) were added as they were recognized in the field in the southern region.

Similar to Grunsky et al. (2009), Harris et al. (2008b), Shelat et al. (2012), LaRocque et al. (2012), and Byatt et al. 2017, representative training areas of each the material classes were delineated from air photo interpretation of the orthorectified Landsat 8 and RADARSAT-2 imagery. Training polygons have at least 10 pixels per class for adequate class representation in the classification (Table 3.5). The training areas were then used to compute class spectral signatures. Landsat-8 OLI data measure the reflective properties of the surficial materials in the visible, near-infrared, and shortwave-infrared wavelengths of the electromagnetic spectrum. These reflective properties are highly related to the presence or absence of vegetation that has a strong reflectance in green (B3) and near-infrared (B5) bands. They are also related to moisture content of surficial materials. The RADARSAT-2 images are related to the backscatter properties in each polarization (HH, HV) of the surficial materials, which depend on surface roughness, morphology (geometry), and moisture content.

Table 3.4. Description of the surficial material classes used in the study for Wager Bay South.

Code	Name	Description
Ap	Alluvial plain	Alluvial sands and minor silts, exposed = periodically water-saturated sediment; alluvial plains, recent deltas and fans; beaches; intertidal flats
Af	Flooded Alluvium	Alluvial sediments (sand and silt deposit) periodically covered by small amount of water
At	Alluvial terrace	Exposed sand and minor silt = sandy sediment; mostly dry; alluvial terraces, former deltas and fans
O	Organic	Organics = saturated thin organic sediments; poor drainage; shallow sedge fens and sphagnum bogs
Mc	Offshore silt and clay	Very fine sediments, essentially silt and clay, deposited in the bottom of a quiet water (glaciomarine or glaciolacustrine)
McV	Offshore silt and clay with vegetation	Very fine sediments, essentially silt and clay, deposited in the bottom of a quiet water (glaciomarine or glaciolacustrine), covered by a vegetation growing on the surface
Ms	Marine sand	Sand and minor silt, exposed or lichen-covered = sediments locally wave-washed or winnowed; thick (> 1 m) marine or minor glaciolacustrine deposits; may include eolian dunes and raised beaches.
MsV	Marine sand with vegetation	Sand and minor silt; covered with short but dense vegetation = sediments locally wave-washed or winnowed; thick (>2 m) marine or minor glaciolacustrine deposits; may include vegetated eolian dunes and raised beaches.
Ms/R	Thin marine sand	Marine sand and minor silt veneer = sediments locally wave-washed or winnowed; thin (< 1 m) marine deposits; bedrock outcrops may appears but cover less than 50% of the surface.
SG	Sand & Gravel	Sand and gravel, exposed or lichen-covered = proglacial deltas, eskers, outwash terraces, ice-contact glaciofluvial deposits, coarse-grained marine beaches and terraces
SGV	Sand & Gravel with vegetation cover	Sand and gravel, covered with short vegetation = proglacial deltas, eskers, outwash terraces, ice-contact glaciofluvial deposits coarse-grained marine beaches and terraces
S/R	Thin sand and gravel over bedrock	Sand and gravel veneer= proglacial deltas, eskers, outwash terraces, ice-contact glaciofluvial deposits, bedrock outcrops may appears but cover less than 50% of the surface.
T	Thick till	Non-bouldery till = silty-sand to silty–clay diamicton; grass- and lichen-covered; includes blanket and streamlined till; commonly soliflucted; thickness commonly > 1 m
bT	Bouldery till	Bouldery till = silty-sand to sandy diamicton; abundant lichen-covered boulders on surface; includes thin (< 1 m) veneers and thick (> 1 m) deposits of, streamlined till, bouldery till blankets, eroded/modified till and/ or wave-washed (winnowed) till.
gT	Gravelly till	Very coarse till, mainly composed of coarse diamicton, particularly gravel
gsT	Gravelly sandy till	Coarse till, mainly composed of sand and gravel diamicton.
sT	Sandy till	Sandy till = sandy diamicton, including eroded till; found with undifferentiated glaciofluvial sediments in meltwater corridor complex; thickness commonly between 2 to 5 m; hummock topography interspersed with eroded till features; grass- and/or lichen-covered.
wT	Wave-washed till	Wave-washed till, wave-washed sandy till; thickness > 30 cm; often covered with a thin layer (< 30 cm) of littoral sediments.
TV	Thick till with dense vegetation cover	Vegetation-covered till = silty-sand to silty–clay diamicton; includes blanket and streamlined till; commonly soliflucted; thickness commonly > 1 m; grass-covered.
T/R	Thin till	Till veneer = silty-sand to sandy diamicton, thin cover interspersed with bedrock outcrops; till thickness commonly < 1 m; bedrock outcrops may appears but cover less than 50% of the surface; may have some boulders; little vegetation.
B	Boulders	Boulders = includes exposed and lichen-covered felsenmeer (broken bedrock) and boulder fields; boulders cover more than 50% of the surface; rare discontinuous till and bedrock.
R	Bedrock	Undifferentiated bedrock = intact and frost-riven exposed outcrops of various lithology; bedrock outcrops cover more than 50% of the surface; surface range from rough and weathered to glacially polished and striated, patches of boulders and thin drift cover; may be show lichen-covered outcrop.

Table 3.5. Characteristics of the training area polygons and number of validation GPS sites per class.

Code	Number of training polygons	Number of pixels	Area (km^2)	Percent of image (%)	Number of validation GPS sites
Ap	4	40	36.0	0.000221	11
Af	8	80	72.0	0.000442	9
At	6	60	54.0	0.000332	9
O	10	111	99.9	0.000614	20
Mc	5	40	36.0	0.000221	14
McV	12	120	108.0	0.000663	33
Ms	15	140	126.0	0.000774	33
MsV	6	60	54.0	0.000332	15
Ms/R	21	200	180.0	0.001105	63
SG	19	182	163.8	0.001006	35
SGV	14	140	126.0	0.000774	29
S/R	4	40	36.0	0.000221	9
T	9	83	74.7	0.000459	31
bT	12	120	108.0	0.000663	39
gT	4	40	36.0	0.000221	13
gsT	4	40	36.0	0.000221	25
sT	11	100	90.0	0.000553	27
wT	13	120	108.0	0.000663	36
TV	10	100	90.0	0.000553	28
T/R	14	140	126.0	0.000774	63
B	8	80	72.0	0.000442	18
R	19	180	162.0	0.000995	88

The accuracy of image classification greatly depends on the spectral separability between classes. In this study, the spectral separability was assessed by the Jeffries-Matusita (J-M) distance, which has values ranging from 0 to 2. A value between 0 and 1 indicates a very poor separation, 1 and 1.9 suggests a moderate separation, and 1.9 and 2.0 reflects a good separation (Richards, 1993).

The classifier used in this study is a non-parametric decision-tree–type classifier (RF), which does not require normal distribution of the input data (Breiman, 2001, 2003). The algorithm used for this study was developed in the R programming language (R Development Core Team, 2012), which had recently been successfully employed in a

study on surficial material mapping in the Hudson Bay Lowland (Ou et al., 2016). The RF classifier has two versions, known as "*all-polygon*" and "*sub-polygon*". The *all-polygon* version uses all of the pixels within all of the training area polygons to define class training areas, whereas the *sub-polygon* version randomly selects a user-determined number of training area pixels from each class. This study only uses the *all-polygon* version; it has the advantage of taking into account the actual class size, and that produces better results, as we showed in the study of the Wager Bay North area (Byatt et al. 2017). The settings of the classifier were the same as for the north Wager Bay study, namely a forest of 500 independent decision trees with the default values for the *mtry* variable, without bootstrapping (Byatt et al. 2017).

For both the J-M distance computation and the classifier, two image combinations were considered: 1) only the Landsat-8 OLI images; and 2) a combination of Landsat-8 OLI and RADARSAT-2 images. In both cases, DEM and derived slope data were included in the classification to take into account topographic (elevation) information of each class. Also, the classifier was applied to the images where background, lakes, rivers, and other water bodies were masked out with a mask that was created from a combination of Landsat 8 B7 (Shortwave infrared) and RADARSAT-2 C-HV images.

3.5.3 Accuracy assessment

Classification accuracy was assessed first by comparing training areas with the equivalent classified land use in the imagery. Such comparison was performed under the form of a "confusion matrix" or error matrix", where each cell expresses the number of pixels classified to a particular class in relation to the class defined by the training areas

(Congalton 1991). The confusion matrix allows computing individual User's and Producer's class accuracies and their related errors (omission and commission), as described in Congalton (1991). The User's class accuracy corresponds to the probability that a pixel of the classified image is in the correct class, the associated number of misclassified pixels being pixels classified in the incorrect class (error of omission). The Producer's accuracy measures the probability that a reference pixel is effectively well classified, the associated number of misclassified pixels being pixels that actually belong to another class (error of commission). From the confusion matrix, it is also possible to compute the average and overall accuracies. The average accuracy was computed as the simple average between User's class accuracies, whereas the overall accuracy is the average of individual class User's or Producer's accuracies, weighted by the size of the class in the classified or reference image.

The aforementioned method gives the classified image accuracy, which is different than the true mapping accuracy. Indeed, a more robust and independent accuracy assessment is to compare the resulting classified image with an independent set of GPS field observation data acquired over the validation sites. If the image returns the same class as the one observed at the validation sites, then the pixel related to this validation site is given a value of 1. If it is not the case, then the value is zero. A confusion matrix between the ground truth and classified image can then be computed. In this study, we used 648 GPS points for validating the resulting map. The distribution of the points among the various classes is presented in Table 3.5.

3.6 RESULTS AND DISCUSSION

3.6.1 J-M Distance

J-M distances were computed to determine the class separability for the Landsat-8 TIM images alone (Table 3.6) or combined with RADARSAT-2 SAR images (Table 3.7). The Landsat-8 images produced decent separabilities, with a mean J-M distance of 1.968. The minimum J-M distance was 1.101 and occurred between *marine sand (Ms)* and *alluvial terrace (At)*. This is consistent with the findings of the study done in the Wager Bay North region (Byatt et al. 2017). There were 16 class pairs that showed a J-M distance of less than 1.85, indicating there is slightly higher separabilities than in the Wager Bay North study, which had 21 class pairs showing a J-M distance of less than 1.85 (Byatt et al. 2017). The minimum values in the northern region were between *marine clay (Mc)* and *alluvial terrace (At)*. This is a similar pairing, both study areas showing low values between a marine sediment and alluvial terrace, however there is a slight difference in the type of sediment (sand vs clay). This difference is probably due to the fact that the training areas used in this study include slightly different surficial classes, as mentioned above. However, similar to Byatt et al. (2017), the minimum J-M distance of 1.101 is still higher than the values of Shelat et al. (2012) (0.75), and LaRocque et al. (2012) (0.50). Each of these studies used Landsat 7 ETM+ images, which do not have the same spectral resolution as the Landsat-8 OLI images. This study also includes images acquired under both wet and dry surface conditions, which have been shown in Byatt (2014) to improve the class separability.

Table 3.6. J-M distances computed for the Landsat-8 OLI images.

Class	Ap	Af	At	O	Mc	McV	Ms	MsV	Ms/R	SG	SGV	S/R	T	bT	gT	gsT	sT	wT	TV	T/R	B
Af	1.990																				
At	2.000	2.000																			
O	2.000	2.000	2.000																		
Mc	1.998	2.000	1.794	2.000																	
McV	2.000	2.000	2.000	1.914	2.000																
Ms	2.000	2.000	1.101	2.000	1.647	2.000															
MsV	2.000	2.000	2.000	1.969	2.000	1.749	2.000														
Ms/R	1.892	2.000	1.995	2.000	1.938	2.000	1.992	2.000													
SG	1.588	1.968	1.943	1.999	1.875	2.000	1.952	2.000	1.736												
SGV	1.966	2.000	2.000	1.994	2.000	2.000	2.000	2.000	1.747	1.891											
S/R	2.000	2.000	2.000	2.000	2.000	2.000	2.000	2.000	2.000	2.000	1.814										
T	2.000	2.000	2.000	1.922	2.000	2.000	2.000	2.000	2.000	2.000	1.999	2.000									
bT	1.995	1.983	1.961	1.952	1.933	2.000	1.966	1.995	1.985	1.818	1.993	2.000	1.675								
gT	2.000	2.000	2.000	2.000	2.000	2.000	2.000	2.000	2.000	1.999	2.000	2.000	2.000	1.989							
gsT	2.000	2.000	2.000	1.996	2.000	2.000	2.000	2.000	2.000	2.000	2.000	2.000	1.999	1.994	2.000						
sT	2.000	2.000	2.000	1.968	2.000	1.799	2.000	2.000	2.000	2.000	2.000	2.000	1.997	1.995	2.000	2.000					
wT	2.000	2.000	2.000	1.995	2.000	1.978	2.000	1.791	1.999	2.000	2.000	2.000	2.000	1.996	2.000	2.000	2.000				
TV	2.000	2.000	2.000	1.842	2.000	1.991	2.000	2.000	2.000	2.000	1.997	2.000	1.990	1.989	2.000	2.000	1.935	2.000			
T/R	1.999	2.000	2.000	1.996	2.000	2.000	2.000	2.000	1.976	1.982	1.677	1.955	2.000	1.998	2.000	2.000	1.999	2.000	1.936		
B	2.000	2.000	2.000	2.000	2.000	2.000	2.000	2.000	2.000	2.000	1.996	2.000	2.000	2.000	2.000	2.000	2.000	2.000	1.993	1.928	
R	1.983	2.000	2.000	1.996	2.000	2.000	2.000	2.000	1.888	1.853	1.543	1.746	1.999	1.994	2.000	2.000	2.000	2.000	1.963	1.424	1.996

J-M distance: Minimum= 1.101; Mean = 1.968; Maximum= 2.000

Table 3.7. J-M distances computed for the Landsat-8 OLI and RADARSAT-2 dual-pol (HH, HV) images.

Class	Ap	Af	At	O	Mc	McV	Ms	MsV	Ms/R	SG	SGV	T	bT	cT	gT	gsT	sT	TV	T/R	B
Af	2.000																			
At	2.000	2.000																		
O	2.000	2.000	1.943																	
Mc	2.000	2.000	1.892	1.956																
McV	2.000	2.000	2.000	2.000	2.000															
Ms	2.000	2.000	1.896	1.905	1.903	2.000														
MsV	2.000	2.000	2.000	2.000	2.000	2.000	2.000													
Ms/R	2.000	2.000	2.000	2.000	2.000	2.000	2.000	2.000												
SG	2.000	2.000	2.000	2.000	2.000	2.000	2.000	2.000	2.000											
SGV	2.000	2.000	2.000	2.000	2.000	2.000	2.000	2.000	2.000	2.000										
T	2.000	2.000	2.000	1.998	2.000	2.000	2.000	2.000	2.000	2.000	2.000									
bT	2.000	2.000	2.000	1.997	2.000	2.000	1.999	2.000	2.000	2.000	1.999	1.983								
cT	2.000	2.000	2.000	2.000	2.000	2.000	1.999	2.000	2.000	2.000	2.000	1.999	1.999							
gT	2.000	2.000	2.000	1.999	2.000	2.000	1.998	2.000	2.000	2.000	2.000	1.999	1.997	2.000						
gsT	2.000	2.000	2.000	1.990	2.000	2.000	1.999	2.000	2.000	2.000	2.000	1.965	1.988	2.000	1.992					
sT	2.000	2.000	2.000	2.000	2.000	2.000	2.000	2.000	1.999	2.000	2.000	1.966	1.999	2.000	2.000	2.000				
TV	2.000	2.000	2.000	2.000	2.000	2.000	2.000	2.000	2.000	2.000	2.000	2.000	2.000	2.000	2.000	2.000	2.000			
T/R	2.000	2.000	2.000	1.999	2.000	2.000	2.000	2.000	1.997	2.000	1.999	1.908	1.975	1.997	1.994	1.960	1.898	2.000		
B	2.000	2.000	2.000	1.999	2.000	2.000	2.000	2.000	2.000	2.000	2.000	1.984	1.996	2.000	1.999	1.991	1.996	2.000	1.857	
R	2.000	2.000	2.000	2.000	2.000	2.000	2.000	2.000	2.000	2.000	2.000	2.000	2.000	2.000	2.000	2.000	2.000	2.000	2.000	2.000

J-M distance: Minimum= 1.961; Mean = 1.999; Maximum= 2.000

Once the RADARSAT-2 SAR images were combined to the Landsat-8 OLI images, the J-M distances increased dramatically. There were no class pairs having a J-M distance of less than 1.95 with most values above 1.99. The mean increased to 1.999 and the minimum to 1.961 between *sand and gravel (SG)* and *thin marine sediment over bedrock (M/R)*. Even the *Marine clay* class did not show any confusion with a value of 2.0 for all class comparisons. This indicates that the addition of RADARSAT-2 data improves substantially the separation between classes. This is consistent with the findings of the study in the Wager Bay North area, which showed a similar increase in J-M distance once the RADARSAT-2 data was added to the image combination (Byatt et al. 2017). The minimum value from the northern region was between *Boulders (B) and Thin till over bedrock (T/R)*. We also observed much higher J-M distances for these classes in the south area than for the north area., probably because of better training area selection, better image quality, or because the considered classes have a higher spectral separability.

3.6.2 Classification accuracies

The overall classification accuracy produced from the Landsat-8 data alone was 96.7% (Table 3.8). This is slightly higher than what was produced from the Wager Bay North study (92.8%) (Byatt et al. 2017). These accuracies are much higher than the classification accuracies produced from comparative studies using Landsat optical data alone over similar northern terrain in Shelat et al. (2012) (80.3%), Grunsky et al. (2006) (84.8%), and LaRocque et al. (2012) (86.2%). It is also much higher than the accuracies produced by Campbell et al. (2013) (46.3%) and Wityk et al. (2013) (62.2%).

Table 3.8. Class accuracies (in %) obtained by applying the Random Forests classifier to a combination of DEM, slope, and image data as a function of the images used in the classification.

Class code	User's accuracy		Producer's accuracy	
	Landsat-8	Landsat-8 & RADARSAT -2	Landsat-8	Landsat-8 & RADARSAT-2
Ap	90.0	95.0	92.3	100
Af	100	100	100	100
At	95.0	100	93.4	100
O	96.3	100	98.1	99.1
Mc	100	100	81.6	100
McV	100	100	97.6	98.4
Ms	97.9	99.3	95.8	98.6
MsV	91.7	96.7	96.5	98.3
Ms/R	97.5	100	97.5	99.0
SG	81.3	96.7	95.5	99.4
SGV	99.3	99.3	92.7	97.2
S/R	97.5	100	97.5	100
T	97.6	98.8	100	100
bT	99.2	100	99.2	100
gT	100	100	97.6	100
gsT	100	100	100	100
sT	99.0	100	98.0	98.0
wT	98.3	99.2	96.7	99.2
TV	97.0	99.0	96.0	100
T/R	100	100	97.9	100
B	100	100	100	100
R	97.8	99.4	97.2	100
Average	**97.1**	**99.2**	**96.4**	**99.4**
Overall	**96.7**	**99.3**	**96.7**	**99.3**

This observed improvement in accuracy could be explained by the use of *Random Forests* as a classifier, as opposed to the *MLC* classifier used by all previous studies (Byatt et al.2017). It could also be caused by the better spectral resolution of Landsat-8 images compared to Landsat5 or Landsat-7 ETM + images used in all previous studies. Similar to Byatt et al. (2017) and in contrast to all the other previous studies, we included slope and DEM data in the classification. Both variables were consistently ranked as the strongest predictors in the *Random Forests* variable importance plot,

paralleling results by Byatt et al. (2017) (Figure 3.4a). The third most important variable was the near-infrared (NIR) band, which was also the case in Byatt et al. (2017). When the RADARSAT-2 data were added to the Landsat-8 data, the overall classification accuracy improved to 99.3%. The resulting classified image is shown in Figure 3.5. The minimum accuracy is related to the *Alluvial plains* class with 95.0% user's accuracy, which is much higher than the minimum value, when Landsat-8 images were used alone (90.0%). The confusion matrix for the best classifier image is presented in Table 3.9. This class was confused with *Marine clay with vegetation* and *Sand and gravel with vegetation*, but the confusion was minimal. Such improvements were already observed in the previous studies, but the observed improvement was better than in Shelat et al. (2012) (84.0%), Grunsky et al. (2006) (91.9%), LaRocque et al. (2012) (90.8%) and in the Wager bay north study of Byatt et al. (2017) (98.1%). This increase in accuracy was explained by the previous authors by the high sensitivity of RADARSAT-2 to surface roughness and to the presence of moisture in the surficial materials. The rankings of importance from this image combination (Figure 3.4b) were similar to the rankings from the Landsat-8 image alone, with slope ranked as the most important data in the classification process followed by Landsat-8 Band 5 (NR). However, the RADARSAT-2 (A2 HV Wet) image was ranked the third most important band in the classification. In fact, all of the RADARSAT-2 bands were highly ranked, with 5 of the Landsat-8 bands being ranked last. This indicates the importance of adding RADARSAT-2 data into the classification process in this particular study area.

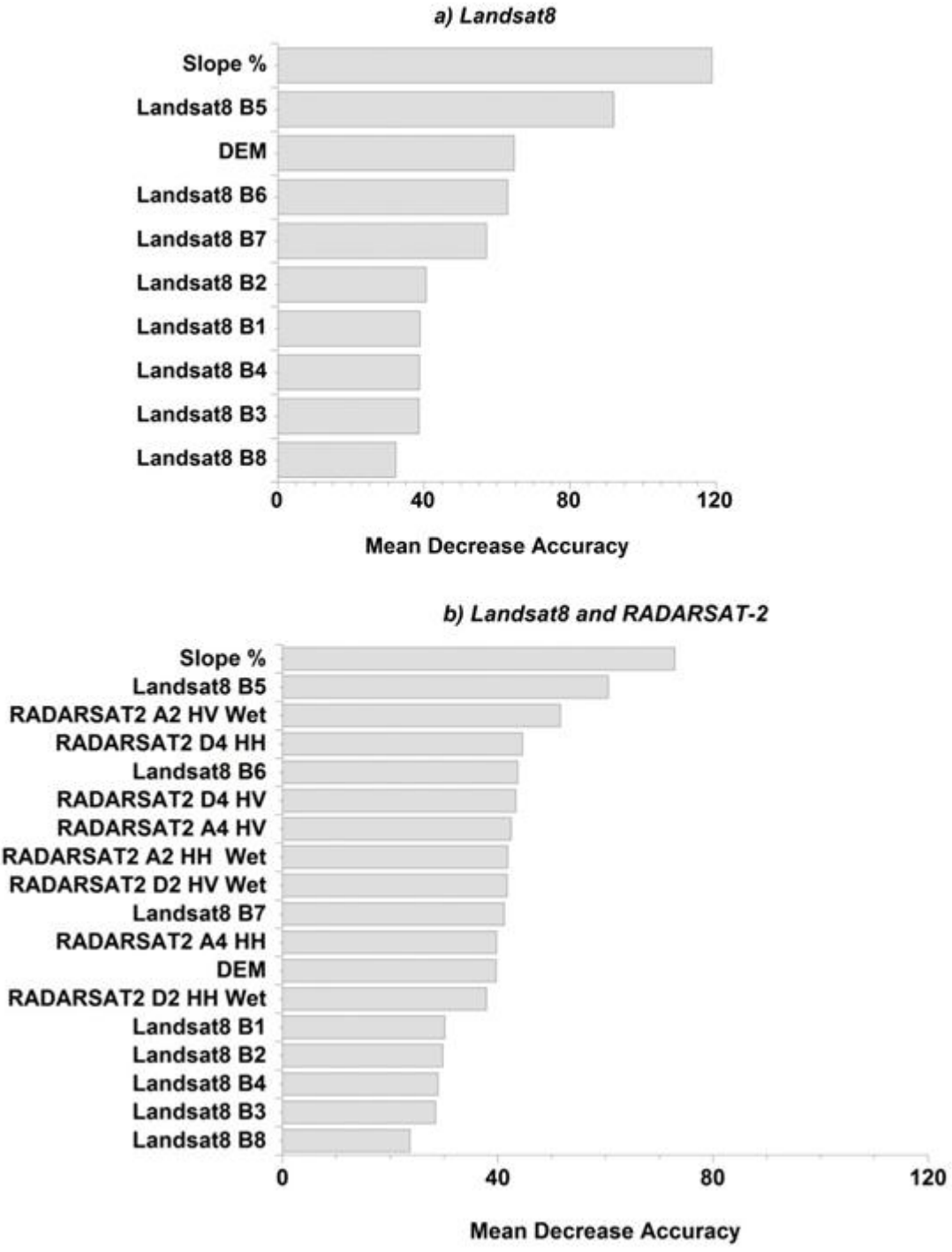

Figure 3.4. Variable importance as produced by the *Random forests* classifier for a) the Landsat-8 classification and b) the Landsat-8 & Radarsat-2 classification.

Table 3.9. Confusion matrix when the Random Forests classifier is applied to the combination of Landsat-8 OLI, RADARSAT-2, DEM, and slope data.

Class	Ap	Af	At	O	Mc	McV	Ms	MsV	Ms/R	SG	SGV	S/R	T	bT	gT	gsT	sT	wT	TV	T/R	B	R	User's Accuracy	Error of Commission
Ap	**38**	0	0	0	0	1	0	0	0	0	1	0	0	0	0	0	0	0	0	0	0	0	95.0	5.0
Af	0	**76**	0	0	0	0	0	0	0	0	0	0	0	0	0	0	0	0	0	0	0	0	100	0.0
At	0	0	**60**	0	0	0	0	0	0	0	0	0	0	0	0	0	0	0	0	0	0	0	100	0.0
O	0	0	0	**109**	0	0	0	0	0	0	0	0	0	0	0	0	0	0	0	0	0	0	100	0.0
Mc	0	0	0	0	**40**	0	0	0	0	0	0	0	0	0	0	0	0	0	0	0	0	0	100	0.0
McV	0	0	0	0	0	**120**	0	0	0	0	0	0	0	0	0	0	0	0	0	0	0	0	100	0.0
Ms	0	0	0	0	0	0	**139**	0	0	1	0	0	0	0	0	0	0	0	0	0	0	0	99.3	0.7
MsV	0	0	0	0	0	1	0	**58**	0	0	0	0	0	0	0	0	0	1	0	0	0	0	96.7	3.3
Ms/R	0	0	0	0	0	0	0	0	**200**	0	0	0	0	0	0	0	0	0	0	0	0	0	100	0.0
SG	0	0	0	0	0	0	2	0	1	**176**	3	0	0	0	0	0	0	0	0	0	0	0	96.7	3.3
SGV	0	0	0	1	0	0	0	0	0	0	**139**	0	0	0	0	0	0	0	0	0	0	0	99.3	0.7
S/R	0	0	0	0	0	0	0	0	0	0	0	**40**	0	0	0	0	0	0	0	0	0	0	100	0.0
T	0	0	0	0	0	0	0	0	0	0	0	0	**82**	0	0	0	1	0	0	0	0	0	98.8	1.2
bT	0	0	0	0	0	0	0	0	0	0	0	0	0	**120**	0	0	0	0	0	0	0	0	100	0.0
gT	0	0	0	0	0	0	0	0	0	0	0	0	0	0	**40**	0	0	0	0	0	0	0	100	0.0
gsT	0	0	0	0	0	0	0	0	0	0	0	0	0	0	0	**40**	0	0	0	0	0	0	100	0.0
sT	0	0	0	0	0	0	0	0	0	0	0	0	0	0	0	0	**100**	0	0	0	0	0	100	0.0
wT	0	0	0	0	0	0	0	1	0	0	0	0	0	0	0	0	0	**119**	0	0	0	0	99.2	0.8
TV	0	0	0	0	0	0	0	0	0	0	0	0	0	0	0	0	1	0	**99**	0	0	0	99.0	1.0
T/R	0	0	0	0	0	0	0	0	0	0	0	0	0	0	0	0	0	0	0	**140**	0	0	100	0.0
B	0	0	0	0	0	0	0	0	0	0	0	0	0	0	0	0	0	0	0	0	**80**	0	100	0.0
R	0	0	0	0	0	0	0	0	1	0	0	0	0	0	0	0	0	0	0	0	0	**179**	99.4	0.6
Producer's Accuracy	100	100	100	99.1	100	98.4	98.6	98.3	99.0	99.4	97.2	100	100	100	100	100	98.0	99.2	100	100	100	100		
Error of Omission	0.0	0.0	0.0	0.9	0.0	1.6	1.4	1.7	1.0	0.6	2.8	0.0	0.0	0.0	0.0	0.0	2.0	0.8	0.0	0.0	0.0	0.0		

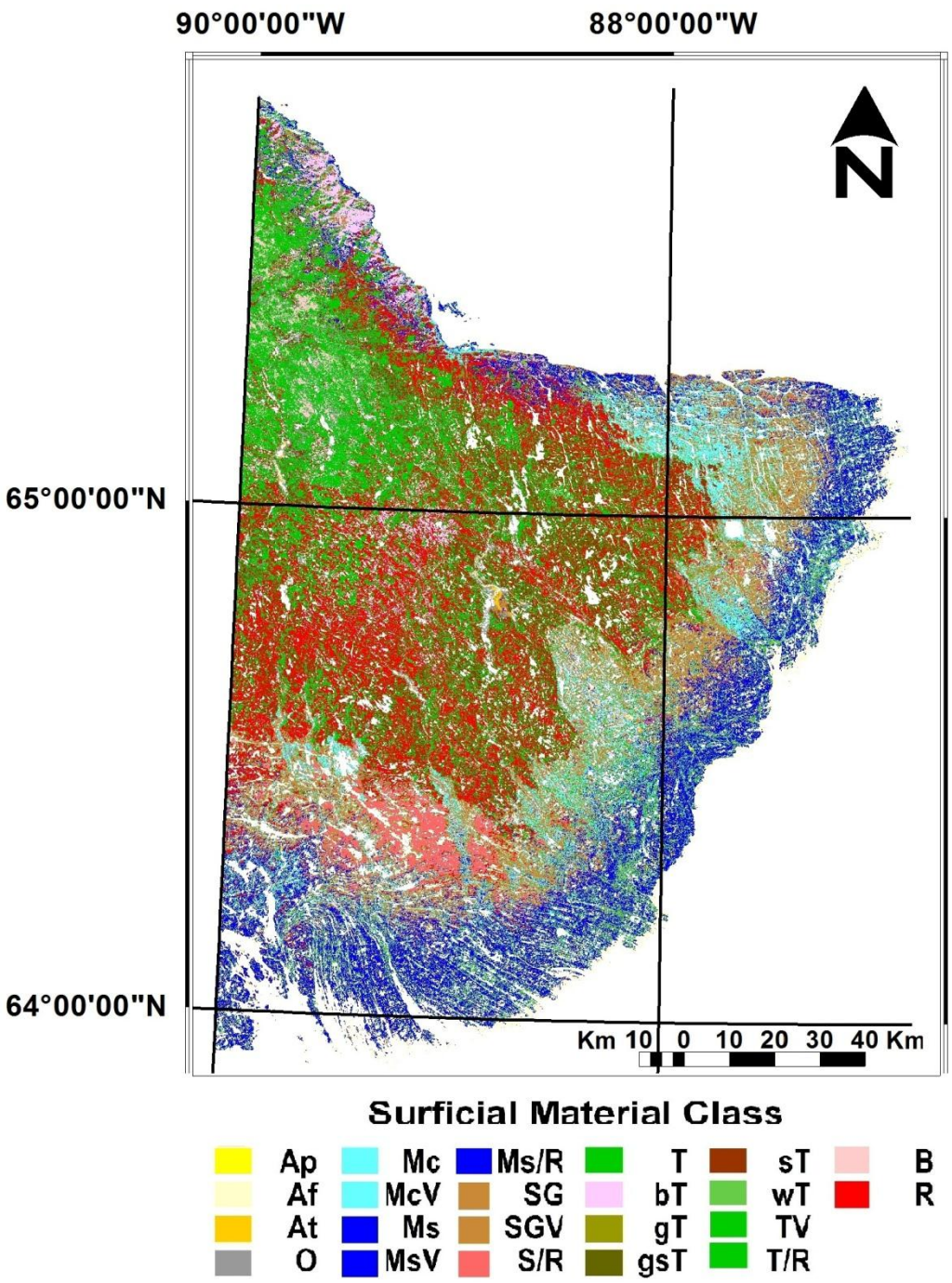

Figure 3.5. Remote predictive surficial materials map for the southern Wager Bay area produced by a Random Forest classifier applied to a combination of Landsat-8, RADARSAT-2 HH / HV, DEM and slope data.

3.6.3 Mapping accuracies

When only the Landsat-8 images are used, the overall mapping accuracy (68.5%) (Table 3.10) was slightly less accurate than for the Wager Bay north region study (76.3%). Only 2 classes scored a perfect 100% mapping accuracy: *flooded alluvium,* and *boulders.* However, in the Wager Bay north region study they only have a mapping accuracy of 80.8% and 87.2%. The maximum accuracy (90.9%) was obtained for the *marine clay with vegetation* class. and *sandy till* classes. Similarly as for the Wager Bay north region study (Byatt et al. 2017), the following classes have a mapping accuracy of less than 80%: *alluvial plains, alluvial terrace, organics, marine clay, marine sediment, thin marine sediment over bedrock, sand and gravel, sand and gravel with vegetation, thin sand and gravel over bedrock, bouldery till, gravelly till, gravelly sandy till, thick till with vegetation, thin till over bedrock,* and *bedrock.*

However, the following classes have a higher mapping accuracy than in the Wager Bay north study (Byatt et al. 2017): *flooded alluvium, alluvial terrace, marine sediment with vegetation, sand and gravel, sand and gravel with vegetation, gravelly sandy till, gravelly till, sandy till, thick till with vegetation,* and *boulders.* The opposite is true for the following classes: *alluvial plains, organics, marine clay, marine clay with vegetation, marine sediments, thin marine sediments over bedrock, till, bouldery till thin till over bedrock,* and *bedrock.* The minimum accuracy (22.2%) occurred with *thin sand and gravel over bedrock,* while for the Wager Bay north study, it was related to the *gravelly till* class (16.7%).

Table 3.10. Ground truth identification accuracies (in %) obtained by comparing the GPS ground observations to the classified image produced by applying the Random Forests classifier to Landsat-8, DEM and slope data, alone or with RADARSAT-2 dual-polarized intensity images (HH and HV).

Class code	User's accuracy		Producer's accuracy	
	Landsat-8	Landsat-8 & Radarsat-2	Landsat-8	Landsat-8 & Radarsat-2
Ap	45.5	63.6	83.3	63.6
Af	100	100	100	90.0
At	55.6	55.6	62.5	83.3
O	45.0	65.0	34.6	59.1
Mc	50.0	78.6	63.6	73.3
McV	90.9	93.9	78.9	81.6
Ms	78.8	78.8	81.3	76.5
MsV	86.7	93.3	81.3	87.5
Ms/R	74.6	85.7	81.0	77.1
SG	71.4	80.0	42.4	60.9
SGV	75.9	82.8	33.3	47.1
S/R	22.2	11.1	40.0	20.0
T	83.9	83.9	72.2	74.3
bT	61.5	69.2	75.0	81.8
gT	69.2	69.2	81.8	75.0
gsT	60.0	84.0	93.8	100
sT	81.5	88.9	88.0	92.3
wT	86.1	88.9	86.1	94.1
TV	78.6	92.9	84.6	86.7
T/R	36.5	54.0	65.7	82.9
B	100	100	90.0	90.0
R	61.4	60.2	70.1	73.6
Average	**68.9**	**76.3**	**72.3**	**75.9**
Overall	**68.5**	**76.1**	**68.5**	**76.1**

When RADARSAT-2 images were added to the classification there was a significant increase in the mapping accuracy (78.0%) (Table 3.11). This was slightly worse than the Wager Bay north study (93.3%) (Byatt et al. 2017). Similarly to the Landsat-8 images alone, the same 2 classes scored a perfect 100% accuracy, *flooded alluvium,* and *boulders.* The classes that have a lower mapping accuracy in this study compared to the Wager Bay north study (Byatt et al. 2017) are *alluvial plain, alluvial terrace, organics,*

marine clay, marine clay with vegetation, marine sediment, sand and gravel, till, boulder till, sandy till, thin till over bedrock, and *bedrock.* The minimum accuracy (11.1%) was found for the *thin sand and gravel over bedrock* class, whereas it was for *gravelly till* (76.7%) in the Wager Bay north region study (Byatt et al. 2017). Indeed, the *thin sand and gravel over bedrock* class was mainly confused with *sand and gravel with vegetation* (6 sites) and *bedrock* (2 sites) (Table 3.11). Interestingly, the *thin sand and gravel over bedrock* class and the *bedrock* class were the only classes to see a decrease in mapping accuracy when the RADARSAT-2 data was added. *Bedrock* saw a decrease of only 1.2%, while *thin sand and gravel over bedrock* saw a decrease of 11.1%. As both classes have bedrock, this could be related to variable bedrock types in the compared GPS sites. However, other bedrock classes in the study did not see such a decrease so it's possibly a random error accentuated by small sample size. While the results are slightly worse in the southern region, they are comparable, and indicate that the methods are applicable to other similar regions in the arctic.

Table 3.11. Confusion matrix (in number of pixels) when comparing GPS ground observations to the classified image produced by applying the Random Forests classifier script to Landsat-8, DEM and slope data, and RADARSAT-2 dual-polarized intensity images (HH and HV).

Class	Ap	Af	At	O	Mc	McV	Ms	MsV	Ms/R	SG	SGV	S/R	T	bT	gT	gsT	sT	wT	TV	T/R	B	R	User's Accuracy	Error of Commission
Ap	**7**	0	0	0	0	0	0	0	0	4	0	0	0	0	0	0	0	0	0	0	0	0	63.6	36.4
Af	0	**9**	0	0	0	0	0	0	0	0	0	0	0	0	0	0	0	0	0	0	0	0	100	0.0
At	0	0	**5**	0	0	0	3	0	0	1	0	0	0	0	0	0	0	0	0	0	0	0	55.6	44.4
O	0	0	0	**13**	0	3	0	0	0	0	1	0	0	0	0	0	0	0	2	1	0	0	65.0	35.0
Mc	0	0	0	0	**11**	0	3	0	0	0	0	0	0	0	0	0	0	0	0	0	0	0	78.6	21.4
McV	0	0	0	0	0	**31**	0	1	0	0	0	0	1	0	0	0	0	0	0	0	0	0	93.9	6.1
Ms	0	0	1	0	0	0	**26**	1	0	5	0	0	0	0	0	0	0	0	0	0	0	0	78.8	21.2
MsV	0	0	0	1	0	0	0	**14**	0	0	0	0	0	0	0	0	0	0	0	0	0	0	93.3	6.7
Ms/R	1	0	0	1	3	1	0	0	**54**	1	0	0	0	0	1	0	0	0	0	0	0	1	85.7	14.3
SG	0	1	0	1	1	0	2	0	0	**28**	1	0	0	0	0	0	0	1	0	0	0	0	80.0	20.0
SGV	0	0	0	0	0	1	0	0	0	0	**24**	0	0	0	0	0	0	0	1	1	1	1	82.8	17.2
S/R	0	0	0	0	0	0	0	0	0	0	6	**1**	0	0	0	0	0	0	0	0	0	2	11.1	88.9
T	0	0	0	0	0	0	0	0	0	0	0	0	**26**	4	0	0	0	0	0	1	0	0	83.9	16.1
bT	0	0	0	1	0	0	0	0	0	0	0	0	8	**27**	0	0	0	0	0	2	1	0	69.2	30.8
gT	0	0	0	1	0	0	0	0	0	1	0	0	0	1	**9**	0	0	0	0	0	0	1	69.2	30.8
gsT	0	0	0	2	0	0	0	0	0	0	0	0	0	1	0	**21**	1	0	0	0	0	0	84.0	16.0
sT	1	0	0	1	0	1	0	0	0	0	0	0	0	0	0	0	**24**	0	0	0	0	0	88.9	11.1
wT	0	0	0	1	0	1	0	0	0	0	0	0	0	0	2	0	0	**32**	0	0	0	0	88.9	11.1
TV	0	0	0	0	0	0	0	0	0	0	0	0	0	0	0	0	0	0	**26**	0	0	2	92.9	7.1
T/R	0	0	0	0	0	0	0	0	4	1	8	2	0	0	0	0	1	1	0	**34**	0	12	54.0	46.0
B	0	0	0	0	0	0	0	0	0	0	0	0	0	0	0	0	0	0	0	0	**18**	0	100	0.0
R	2	0	0	0	0	0	0	0	12	5	11	2	0	0	0	0	0	0	1	2	0	**53**	60.2	39.8
Producer's Accuracy	63.6	90.0	83.3	59.1	73.3	81.6	76.5	87.5	77.1	60.9	47.1	20.0	74.3	81.8	75.0	100	92.3	94.1	86.7	82.9	90.0	73.6		
Error of Omission	36.4	10.0	16.7	40.9	26.7	18.4	23.5	12.5	22.9	39.1	52.9	80.0	25.7	18.2	25.0	0.0	7.7	5.9	13.3	17.1	10.0	26.4		

3.7 CONCLUSIONS

We produced a surficial materials map with 22 classes for an area located south of Wager Bay, Nunavut (NTS map sheets 046D, E, 055P, 056A, H) using a non-parametric classifier, Random Forests (RF), applied to a combination of RADARSAT-2 C-band dual- polarized (HH and HV) and Landsat-8 OLI images with a digital elevation model and slope data. The addition of RADARSAT-2 C-HH and C-HV images to the classification greatly increased the overall classification accuracies from 96.7% when Landsat-8 images were used alone, to 99.3% when RADARSAT-2 C-HH and C-HV images were added.

For most of the individual classes, the user's and producer's accuracy increased when the RADARSAT-2 images were added to the classification, leading to a class accuracy higher than 95% in most of the cases. This increase in accuracy shows the importance of including the RADARSAT-2 into the classification. The classes not mapped with 100% accuracy are *Alluvial plain, Marine sediment, Marine sediment with vegetation, Sand and gravel, Sand and gravel with vegetation, Till, Weathered till, Thick till with vegetation,* and *Bedrock.*

The resulting maps were compared to 648 georeferenced sites with field observations or interpreted from aerial photographs/Google Earth to determine the mapping accuracy. It increased from 68.5% when Landsat-8 images were used alone to 76.1% when RADARSAT-2 images were added. The general increase in accuracies, both classification and mapping, indicates the importance of adding RADARSAT-2 data. The type of RADARSAT-2 data used in this study is limited to images with an incidence angle between 20 and 49.3°, and only C-HH and C-HV bands. The work of Shelat et al

(2012) showed the importance of including a variety of incidence angles (shallow, medium, and steep) in surficial material mapping, as it can increase class separability and classification accuracies. The inclusion of adding VH and VV images could also increase the classification accuracy, as it would add in more data for the classification process to work with. There is also the possibility of including polarimetric data, which can be derived from RADARSAT-2, to examine the potential of this new data source in mapping surficial materials.

3.8 REFERENCES

Breiman, L. 2001: Random forests; Machine Learning, 45(1), 5–32.

Breiman, L. 2003: Manual of setting up, using and understanding random forests, V4.0; University of California Berkeley, Berkeley, California, 33 p., URL <http://www.stat.berkeley.edu/~breiman/Using_random_forests_v4.0.pdf> [November 2015].

Brown, O., Harris, J.R. and Utting, D. 2008: Case study 6: surficial mapping of northern Baffin Island using Landsat and topographic data; *in* Remote Predictive Mapping: An Aid for Northern Mapping, J.R. Harris (ed.), Geological Survey of Canada, Open File 5643, p. 225–232.

Byatt, J. 2014: Influence of environmental conditions on surficial deposit mapping using Landsat-5 TM and RADARSAT-2 polarimetric SAR images; B.Sc. (honour) thesis, University of New Brunswick, Fredericton, New Brunswick, 24 p.

Byatt, J., LaRocque, A., Leblon, B., Harris, J., and McMartin, I. 2017. Mapping surficial materials in Nunavut using RADARSAT-2 C-HH and C-HV, Landsat-8 OLI, DEM, and slope data. Part 1 - North of Wager Bay area, International Journal of Remote Sensing (submitted)

Campbell, J.E., Harris, J.R., Huntley, D.H., McMartin, I., Wityk, U., Dredge, L.A. and Eagles, S. 2013: Remote predictive mapping of surficial earth materials: Wager Bay north area, Nunavut - NTS 46-E (N), 46-K (SW), 46-L, 46-M (SW), 56-H (N), 56-I and 56-J (S); Geological Survey of Canada, Open File 7118, 42 p.

Dredge, L.A., McMartin, I., and Campbell, J.E., 2013a. Reconnaissance surficial geology, Yellow Bluff (west), Nunavut, NTS 46D, West; Geological Survey of Canada, CGM map 145, 1:100,000 scale.

Dredge, L.A., McMartin, I., and Campbell, J.E., 2013b. Reconnaissance surficial geology, Daly Bay (south) and Cape Fullerton (north), Nunavut, NTS 56-A, South and 55-P, North; Geological Survey of Canada, CGM map 146, 1:100,000 scale.

Dredge, L.A., McMartin, I., and Campbell, J.E., 2013c. Reconnaissance surficial geology, Daly Bay (north), Nunavut, NTS 56-A, North; Geological Survey of Canada, CGM map 147, 1:100,000 scale.

Evans, D.L., Farr, T.G., Ford, J.P., Thompson, T.W., and Werner, C.L. 1986. Multipolarization radar images for geologic mapping and vegetation discrimination. IEEE Transactions on Geoscience and Remote Sensing, Vol. GE-24, No. 2, pp. 246□257. doi: 10.1109/TGRS.1986.289644.

Goodman J.W. 1976: Some fundamental properties of speckles; Journal of Optical Society of America, 66(11), 1145–1150.

Google 2015: Google Maps™ satellite image of Wager Bay, Nunavut; Google, image, URL <http://maps.google.ca/maps> [©2015 Google - Imagery, ©2015 Data SIO, NOAA, US Navy, NGA, GEBCO, Landsat, IBCAO Map data, November 2015].

Grunsky, E., Harris, J.R. and McMartin, I. 2009: Predictive mapping of surficial materials, Schultz Lake area (NTS 66 A), Nunavut, Canada; Reviews in Economic Geology, 16, 177–198.

Harris, J.R., Grunsky, E. and McMartin, I. 2008a: Classification of remotely sensed imagery for surficial geological mapping in Canada's north, Case 7; in Remote Predictive Mapping: An Aid for Northern Mapping, J.R. Harris (ed.), Geological Survey of Canada, Open File 5643, p. 233–244.

Harris, J.R., Grunsky, E. and Singhroy, V. 2008b: Radar remote sensing; *in* Remote Predictive Mapping: An Aid for Northern Mapping, J.R. Harris (ed.), Geological Survey of Canada, Open File 5643, p. 135–160.

Harris, J.R., Wickert, L., Lynds, T., Behnia, P., Rainbird, R., Grunsky, E., McGregor, R. and Schetselaar, E. 2011: Remote predictive mapping 3. Optical remote sensing – a review for remote predictive mapping in northern Canada; Geoscience Canada, v. 38, p. 49–83.

LaRocque, A., Leblon, B., Harris, J.R., Jefferson, C.W., Tschirhart, V. and Shelat, Y. 2012: Surficial materials mapping in Nunavut, Canada, with multi-beam

RADARSAT-2 dual-polarization C-HH and C-HV, Landsat-7 ETM+, and DEM data; Canadian Journal of Remote Sensing, 38, 281–305.

McMartin, I. and Dredge, L.A. 2005: History of ice flow in the Shultz Lake and Wager Bay areas, Kivalliq Region, Nunavut; Geological Survey of Canada, Current Research 2005-B2, 10 p.

McMartin, I., Wodicka, N., Bazor, D., and Boyd, B., 2013. Till composition across the Rae craton south of Wager Bay, Nunavut: results from the Geo-mapping Frontiers' Tehery-Cape Dobbs project; Geological Survey of Canada, Open File 7417.

McMartin, I., Campbell, J.E., Dredge, L.A., LeCheminant, A.N., McCurdy, M.W., and Scromeda, N., 2015a. Quaternary geology and till composition north of Wager Bay, Nunavut: results from the GEM Wager Bay Surficial Geology Project; Geological Survey of Canada, Open File 7748, 58 p.

McMartin, I., Byatt, J., Randour, I., and Day, S.J.A., 2015b. Report of 2015 activities for regional surficial mapping, till and stream sediment sampling in the Tehery-Wager GEM 2 Rae Project area; Geological Survey of Canada, Open File 7966.

McMartin, I., Day, S.J.A., Randour, I., Roy, M., Byatt, J.,LaRocque, A. and Leblon, B., 2016. Report of 2016 activities for the surficial mapping and sampling surveys in the Tehery-Wager GEM-2 Rae Project area; Geological Survey of Canada, Open File 8134.

Mei, S. and Paulen, R.C. 2009: Using multi-beam RADARSAT-1 imagery to augment mapping surficial geology in northwest Alberta, Canada; Canadian Journal of Remote Sensing, 35, 1–22.

Ou, C., LaRocque, A., Leblon, B. Yu, Z., Webster, K., McLaughlin, J. 2016: Mapping permafrost using RADARSAT-2 and Landsat images, 2 – Regional mapping, International Journal of Remote Sensing, 37(12): 2751-2779

R Development Core Team 2012: R: a language and environment for statistical computing; software development tools, R Foundation for Statistical Computing, Vienna, Austria, URL <http://www.R-project.org/> [November 2015].

Randour, I. and McMartin, I. in press. Surficial geology, Douglas Harbour (south), Nunavut, NTS 56-H, South; Geological Survey of Canada, CGM map 312, 1:100,000 scale.

Schaber, G.G., McCauley, J.F., and Breed, C.S. 1997. The use of multi- frequency and polarimetric SIR-C/X SAR data in geologic studies of Bir Safsaf, Egypt. Remote Sensing of Environment, Vol. 59, pp. 337□363. doi: 10.1016/S0034-4257(96)00143-5.

Schetselaar, E.M., Harris, J.R., Lynds, T. and de Kemp, E.A. 2007: Remote predictive mapping 1. Remote predictive mapping (RPM): a strategy for geological mapping of Canada's north; Geoscience Canada, 34, p. 93–111.

Shelat, Y., Leblon, B., LaRocque, A., Harris J., Jefferson, C. W., Lentz, D., and Tschirhart, V. 2012b. Effects of incidence angles and image combinations on mapping accuracy of surficial materials in the Umiujalik Lake area, Nunavut using RADARSAT-2, polarimetric and Landsat 7 images, and DEM data. Part 1. Non-Polarimetric Analysis. Canadian Journal of Remote Sensing, 38(3): 383-403

United States Geological Survey 2015: Landsat 8 (L8) data users handbook; Sioux Falls, South Dakota, EROS, June 2015, 9 p., URL <https://landsat.usgs.gov/documents/Landsat-8DataUsersHandbook.pdf> [November 2015].

Wityk, U., Harris, J.R., McMartin, I., Campbell, J.E., Ross, M., and Grunsky, E., 2013. Remote predictive mapping of surficial materials, West of Repulse Bay, Nunavut (NTS 46M-SW, 46L-W and -S, 46K-SW), GSC Open File 7357, 20 pages and appendices

CHAPTER 4

CONCLUSIONS

In this thesis a surficial materials map with 21 classes in the northern Wager Bay region and 22 classes in the southern Wager Bay region was produced. The first objective of this thesis was to assess the potential of a combined use of RADARSAT-2 (C-HH and C-HV) images, Landsat-8 OLI images, slope, and elevation data for mapping surficial materials in Nunavut and to assess the mapping accuracy with GPS field observations. We hypothesized that the combination of these data sets would produce a better classified image with a higher mapping accuracy than Landsat-8 alone. The study Campbell et al (2013), which was a similar remote sensing study on the surficial materials in the Wager Bay north area, used only Landsat optical data and showed a low classification accuracy. We have improved on this accuracy substantially, with an overall classification accuracy of 92.8% for the northern region and 98.1% for the southern region. This improvement shows the importance of including RADARSAT-2 images from both descending and ascending orbits, acquired in wet and dry dates into the classification process.RADARSAT-2 data is sensitive to surface moisture, which can be a good parameter to differentiate surface materials. Also the use of both wet and dry dates was an additional improvement, as Byatt (2014) already showed that using both wet and dry dates strongly improves the accuracy of surficial material maps. RADARSAT-2 data also reach deep layers, whereas optical satellites such as Landsat-8 data only reach the surficial layers. RADARSAT-2 provides information on a thicker surface layer, which can be all useful for differentiating surface materials. RADARSAT-

2 data finally is sensitive to surface roughness and grain size, both variables being important for differentiating between different types of surface materials.

The current thesis was limited to the use of HH and HV polarized images acquired in the C-band. RADARSAT-2 can also provide both VH and VV polarized images, which have been shown (i.e. Shelat et al 2012a) to improve the classification accuracy. Polarimetric RADARSAT-2 data are also available. Following the work of Shelat et al. (2012b), it could be potentially interesting to test the use of polarimetric RADARSAT-2 images for surficial materials mapping, as well as the SAR images taken in longer wavelengths, as provided by ALOS-PALSAR-2 L-band. The inclusion of a diverse data set could prove useful in more accurate surficial materials mapping, and RADARSAT SAR data has been shown in this study to have significant value.

The second objective was to assess the use of *Random forests* (RF) as a classifier. The more common classifier used in surface material classification studies such as in Campbell et al. (2013) and Wityk et al. (2013) has been the *Maximum Likelihood Classifier* (MLC). This thesis shows robustness of the RF classifier that led to higher classification accuracies compared with the studies using MLC. The RF classifier can handle both Gaussian and non Gaussian data, and has no upper limit on the amount of input data. In addition, the RF classifier produces a useful ranking of the importance of the input data in the classification.

REFERENCES

Byatt, J. 2014: Influence of environmental conditions on surficial deposit mapping using Landsat-5 TM and RADARSAT-2 polarimetric SAR images; B.Sc. (honour) thesis, University of New Brunswick, Fredericton, New Brunswick, 24 p.

Campbell, J.E., Harris, J.R., Huntley, D.H., McMartin, I., Wityk, U., Dredge, L.A. and Eagles, S. 2013: Remote predictive mapping of surficial earth materials: Wager Bay north area, Nunavut - NTS 46-E (N), 46-K (SW), 46-L, 46-M (SW), 56-H (N), 56-I and 56-J (S); Geological Survey of Canada, Open File 7118, 42 p.

Shelat, Y., Leblon, B., LaRocque, A., Harris J., Jefferson, C. W., Lentz, D., and Tschirhart, V. 2012a. Effects of incidence angles and image combinations on mapping accuracy of surficial materials in the Umiujalik Lake area, Nunavut using RADARSAT-2, polarimetric and Landsat 7 images, and DEM data. Part 1. Non-Polarimetric Analysis. Canadian Journal of Remote Sensing, 38(3): 383-403

Shelat, Y., Leblon, B., LaRocque, A., Harris J., Jefferson, C. W., Lentz, D., and Tschirhart, V. 2012b. Effects of incidence angles and image combinations on mapping accuracy of surficial materials in the Umiujalik Lake area, Nunavut using RADARSAT-2, polarimetric and Landsat 7 images, and DEM data. Part . Polarimetric Analysis. Canadian Journal of Remote Sensing, 38(3): 404-423

Wityk, U., Harris, J.R., McMartin, I., Campbell, J.E., Ross, M., and Grunsky, E., 2013. Remote predictive mapping of surficial materials, West of Repulse Bay, Nunavut (NTS 46M-SW, 46L-W and -S, 46K-SW), GSC Open File 7357, 20 pages and appendices

VITA

Candidate's full name:

Justin Thomas Bezanson Byatt

Universities Attended:

University of New Brunswick (2014-2017) MScF
University of New Brunswick (2011-2014) BSc ENR
Mount Allison University (2004-2009) BSc

Publication:

Byatt, J., LaRocque, A., Leblon, B., Harris, J., and McMartin, I. 2017. Mapping surficial materials in Nunavut using RADARSAT-2 C-HH and C-HV, Landsat-8 OLI, DEM, and slope data. Part 1 - North of Wager Bay area, International Journal of Remote Sensing (submitted)

Byatt, J., LaRocque, A., Leblon, B., Harris, J., and McMartin, I. 2017. Mapping surficial materials in Nunavut using RADARSAT-2 C-HH and C-HV, Landsat-8 OLI, DEM, and slope data. Part 2 - South of Wager Bay area, International Journal of Remote Sensing (submitted)

Conference Presentations:

Mapping surficial materials north of Wager Bay, Nunavut, using RADARSAT-2 C-HH and C-HV, Landsat-8 OLI, DEM and slope data. Byatt, J., LaRocque, A., Leblon, B., Harris, J., and McMartin, I. Oral presentation and discussion at the 2016 Canadian Association of Geographers Conference, in Halifax, Nova Scotia, Canada, 30 May - 4 June 2016.

Influence of the Environmental Conditions on Surficial Mapping Using Landsat-5 TM and RADARSAT-2 Polarimetric SAR Images. Byatt, J., LaRocque, A., Leblon, B., Harris, J., and McMartin, I. Oral presentation and discussion at the36th Canadian Symposium on Remote Sensing: exploring Synergies, St. John's, Newfound Land, Canada, 8-11 June 2015.